R. & M. No. 3119
(19,922)
A.R.C. Technical Report

R. & M. No. 3119

MINISTRY OF AVIATION

AERONAUTICAL RESEARCH COUNCIL
REPORTS AND MEMORANDA

The Theoretical Evaluation of the Downwash behind Jet-Flapped Wings

By A. J. Ross, Ph.D.

LONDON: HER MAJESTY'S STATIONERY OFFICE
1961
PRICE 12*s.* 6*d.* NET

The Theoretical Evaluation of the Downwash behind Jet-Flapped Wings

By A. J. Ross, Ph.D.

Communicated by the Director-General of Scientific Research (Air)
Ministry of Supply

*Reports and Memoranda No. 3119**
January, 1958

Summary. The downwash behind jet-flapped wings of infinite and finite span has been evaluated, using the solutions given by Spence[1] and Maskell[2] for the flow in two and three dimensions respectively. The wing incidence and jet deflection are assumed to be small, and the displacement of the jet is taken into account by displacing the downwash field so that the relative distance between the jet and tailplane is correct. It is also assumed that the spanwise loading on the finite wing is elliptic, and that the trailing vorticity is generated at one particular chordwise position. The wake is considered to be a flat sheet, and so the effect of the rolling-up of the wake has been neglected.

Charts are given for the functions required in the calculation of the downwash for four specific values of jet momentum coefficient. Results have been obtained for the infinite wing and for a wing of aspect ratio 6·0, for various tailplane positions, and varying wing incidence, jet deflection and jet momentum coefficient. A comparison is also made with some American experimental results[5] for a wing of aspect ratio 8·4, and the agreement is good, especially when the experimental lift coefficient is used in the calculations (since it differs considerably from the theoretical lift value, owing to the fact that the experimental wing has a blown flap).

Introduction. When considering the design of a jet-flapped aircraft from a stability and control aspect, it is necessary to have fairly accurate information concerning the downwash field behind the jet-flapped wing, particularly in those regions where it is practicable to locate the tailplane. The evaluation of the downwash at the tailplane is dependent upon a knowledge of the strength and position of the vorticity distributions which represent the wing and the jet. In his treatment of the flow past a wing with a jet-flap, of infinite span, Spence[1] assumes that the incidence of the wing and the deflection of the jet are small, and hence the usual assumptions of thin aerofoil theory, in which the wing and jet are replaced by vortex sheets in the direction of the free stream, apply. The results so obtained for the vorticity distributions on the wing and jet are used in Part I to give the downwash at any position relative to the plane vortex sheet in the form

$$\epsilon = \frac{\partial \epsilon}{\partial \tau}\tau + \frac{\partial \epsilon}{\partial \alpha}\alpha ,$$

where ϵ = downwash angle, τ = jet deflection angle, and α = wing incidence. However, in the calculation of the downwash induced at a point (P) in the field, it is necessary to allow for its location relative to the actual wing and jet. To the order of accuracy consistent with the previous assumptions, this implies calculating the downwash at a point whose ordinate relative to the plane

* R.A.E. Report Aero. 2599, received 13th March, 1958.

vortex sheets is equal to the distance of the tailplane from the jet (as shown in Figs. 1a and 1b). The functions $\partial\epsilon/\partial\tau$ and $\partial\epsilon/\partial\alpha$ depend upon the jet momentum coefficient C_J, and on the relative position of the tailplane; charts for these functions, and for the position of the jet, are given for various specific C_J values. The downwash has been evaluated for ranges of the tailplane position, wing incidence, jet deflection and jet momentum coefficient.

For the unswept wing of finite span, with a full-span jet-flap, considered in Part II, Maskell[2] has introduced the concept of an effective wing and jet flap of infinite span, in order to obtain the strength of the bound vorticity, elliptic spanwise loading being assumed. This solution may be used to give the contribution to the downwash from the bound vorticity, in a similar way to that described in Part I, but it does not account for the effect of the trailing vortices arising from the pressure gradients along the wing and jet spans. In the case of a wing without a jet-flap, it has been found[3] that the downwash is very sensitive to the relative distance between the tailplane and the wake, and that the spanwise loading has more effect on the downwash than the chordwise loading, and so the wing and its wake are replaced by a lifting line and its trailing vortices, the latter being displaced in order to keep the tailplane at the correct height above the wake. The effect of the rolling-up of the wake has also been investigated[6] for a wing without a jet-flap, and it is shown that rolling-up is not important for normal tailplane positions behind wings of large aspect ratio. The distance e behind the wing at which rolling-up may be assumed to be complete is given by $e/c = k'/C_L$ for a wing without a jet-flap, where k' depends upon the plan-form and spanwise loading of the wing. For the jet-flapped wing, the C_L will be greater than for the normal wing, but k' may now be a function of C_J, and will probably increase with increasing C_J (since the bound vorticity on the jet will tend to resist rolling-up), so that e/c will not decrease so quickly with increasing C_L and C_J, as might have been expected from first considerations. Thus, in order to evaluate the contribution to the downwash behind a jet-flapped wing from the trailing vorticity, it is assumed that the majority of the load is carried on the wing, so that the trailing vortices may be considered to arise from one chordwise position on the wing, with no rolling-up taking place. The displacement of the jet and trailing vortices is accounted for by taking the position of the tailplane relative to the wake, and a chart is given for the downwash due to the trailing vorticity. Calculated values of the downwash are in good agreement with the few experimental results available[5], especially if the difference between the experimental and theoretical lift coefficients is taken into account. Theoretical results for the downwash on the centre-line are also given for a wing of aspect ratio 6·0, showing variation with tailplane position, wing incidence, and jet parameters.

PART I

1. *Vortex Representation of the Wing and Jet-Flap of Infinite Span.* The wing and jet-flap of infinite span may be represented in two dimensions by vorticity distributed on the chordal plane of the wing and the median line of the jet (assumed to be thin). The downwash relations have been solved by Spence[1], using the assumptions of thin-aerofoil theory, so that the aerofoil incidence and jet deflection are considered to be small. The vorticity distributions and the position of the jet are given in Fourier-series forms, with coefficients as functions of the jet momentum coefficient C_J.

Let $U_0 f(x)$ be the vorticity distribution on the aerofoil (at incidence α to the mainstream) and $\gamma(x)$ the vorticity distribution on the jet (emerging at deflection τ to the extended chord-line of the aerofoil), as shown in Fig. 1a. The x axis is taken parallel to the main stream, and the z axis vertically downwards, with the origin at the leading edge of the aerofoil. The chord of the aerofoil

is taken to be unity, so that x and z are non-dimensional. Thus the vortex representation of the flow which is in accordance with the assumptions of thin aerofoil theory is as shown in Fig. 1b, with $U_0 f(x)$ located on the x axis, between 0 and 1, and $\gamma(x)$ also on the x axis, between 1 and ∞.

Then the expressions for $f(x)$, $\gamma(x)$ and $z_J(x)$, the jet displacement, as obtained from Ref. 1, are:

For

$$0 < x < 1, \qquad x = \tfrac{1}{2}(1 - \cos\theta) \tag{1}$$

$$f(x) = \frac{2\tau}{x^{3/2}}\left\{-\frac{1}{\pi}\log(1-x) + A_0\left(1-\cos\frac{\theta}{2}\right) + \sum_{n=1}^{N-1} A_n\left(\tan\frac{\theta}{4}\right)^{2n}\right\}$$

$$+ \frac{2\alpha}{x^{3/2}}\left\{x(1-x)^{1/2} + B_0\left(1-\cos\frac{\theta}{2}\right) + \sum_{n=1}^{N-1} B_n\left(\tan\frac{\theta}{4}\right)^{2n}\right\}. \tag{2}$$

For

$$1 < x < \infty, \qquad x = \sec^2\frac{\phi}{2} \tag{3}$$

$$z_J = \tau\left[2\left(1-\cos\frac{\phi}{2}\right) + A_0\left\{\log\left(\frac{1+\sin\frac{\phi}{2}}{1-\sin\frac{\phi}{2}}\right) - 2\sin\frac{\phi}{2}\right\}\right.$$

$$\left. + \sum_{n=1}^{N-1}\frac{A_n}{(4n^2-1)}\left(2\cos\frac{\phi}{2}\sin n\phi - 4n\sin\frac{\phi}{2}\cos n\phi\right)\right]$$

$$+ \alpha\left\{\frac{1}{1+\sin\frac{\phi}{2}} + (B_0 + \tfrac{1}{2})\log\left(\frac{1+\sin\frac{\phi}{2}}{1-\sin\frac{\phi}{2}}\right) - 2B_0\sin\frac{\phi}{2}\right.$$

$$\left. + \sum_{n=1}^{N-1}\frac{B_n}{(4n^2-1)}\left(2\cos\frac{\phi}{2}\sin n\phi - 4n\sin\frac{\phi}{2}\cos n\phi\right)\right\} \tag{4}$$

$$\frac{\gamma(x)}{U_0} = \tau\left\{-\frac{4}{\pi}\cos^3\frac{\phi}{2}\log\left(\tan\frac{\phi}{2}\right) + 2\cos^3\frac{\phi}{2}\sum_{n=0}^{N-1} A_n\cos n\phi\right\}$$

$$+ \alpha\left\{2\cos^3\frac{\phi}{2}\sum_{n=0}^{N-1} B_n\cos n\phi\right\}. \tag{5}$$

2. *The Downwash.* The downwash induced by the vortex distributions $U_0 f(x)$ and $\gamma(x)$ at the point (X, Z) is given by

$$w(X, Z) = \frac{1}{2\pi}\left\{\int_0^1 \frac{U_0 f(x)(X-x)}{(X-x)^2 + Z^2}\,dx + \int_1^\infty \frac{\gamma(x)(X-x)}{(X-x)^2+Z^2}\,dx\right\} \tag{6}$$

to the first order in α and τ (*see* Fig. 1b).

In order to apply the results calculated for the simplified configuration (Fig. 1b) to the actual configuration (Fig. 1a), where the jet is displaced a distance $z_J(X)$ below the x axis, it is assumed that the downwash $w(X, z)$ calculated for the point $P'(X, z)$ in Fig. 1b is equal to the downwash at the point $P(X, z + z_J)$ in Fig. 1a.

A similar procedure is followed in Ref. 3, where the displacement of the wake of a finite wing has to be considered.

In general, the tailplane will be located a distance H above the jet, as indicated in Fig. 1a, so that to evaluate the downwash at the tailplane, *i.e.*, at the point $(X, z_J - H)$ in Fig. 1a, we must evaluate the downwash at the point $(X, -H)$ in Fig. 1b.

The position of the tailplane is usually given as the distance along and height above the extended chordline. If l is the distance of the aerodynamic centre of the tailplane behind the wing leading edge, measured along the extended wing chord-line, and h the height above the chord-line, when the chord is of length c, as shown in Fig. 1a, then the non-dimensional co-ordinates (X, Z) at which the downwash is to be evaluated are given by

$$X = \frac{l}{c} + \frac{h}{c}\alpha\,, \tag{8a}$$

$$Z = -H = \frac{l}{c}\alpha - \frac{h}{c} - z_J(X)\,, \tag{8b}$$

where z_J may be obtained from Fig. 3* (or equation (4)).

For the numerical evaluation of the two integrals in equation (6), it is necessary to change the variables of integration, in the first integral using equation (1) in order to avoid the infinite value of $f(x)$ at the leading and trailing edges, and in the second integral using equation (3) to make the range of integration finite. Thus, if we write

$$\left.\begin{aligned} f(x) &= f_1(x)\tau + f_2(x)\alpha \\ \frac{\gamma(x)}{U_0} &= \gamma_1(x)\tau + \gamma_2(x)\alpha \end{aligned}\right\}, \tag{9}$$

then the downwash at the tailplane is given by

$$w = \frac{U_0}{2\pi}\tau\left[\int_0^\pi \frac{f_1(x)\,\frac{1}{2}\sin\theta(X-x)}{(X-x)^2+Z^2}\,d\theta + \int_0^\pi \gamma_1(x)\,\frac{\sin\frac{\phi}{2}}{\cos^3\frac{\phi}{2}}\,\frac{(X-x)}{\{(X-x)^2+Z^2\}}\,d\phi\right]$$

$$+ \frac{U_0}{2\pi}\alpha\left[\int_0^\pi \frac{f_2(x)\,\frac{1}{2}\sin\theta(X-x)}{(X-x)^2+Z^2}\,d\theta + \int_0^\pi \gamma_2(x)\,\frac{\sin\frac{\phi}{2}}{\cos^3\frac{\phi}{2}}\,\frac{(X-x)}{\{(X-x)^2+Z^2\}}\,d\phi\right], \tag{10}$$

where $f_1(x)\sin\theta$ and $f_2(x)\sin\theta$ remain finite as x and θ tend to zero, and as $x \to 1$, $\theta \to \pi$. Equation (10) may be rewritten in the form

$$\frac{w}{U_0} = \epsilon = \frac{\partial\epsilon}{\partial\tau}\tau + \frac{\partial\epsilon}{\partial\alpha}\alpha\,, \tag{11}$$

where $\partial\epsilon/\partial\tau$ and $\partial\epsilon/\partial\alpha$ are functions of C_J, X and Z. These have been evaluated for $C_J = 0{\cdot}5$, $1{\cdot}0$, $2{\cdot}0$ and $4{\cdot}0$, with $3 < X < 5$ and $0 < |Z| < 3$, the results being shown as charts in Figs. 4a to 4d.

---

* The suffix $_e$ on C_J and α refer to the finite-wing case considered in Part II. For infinite aspect ratio, $\alpha_e \equiv \alpha$ and $C_{Je} \equiv C_J$ in Fig. 3 and Figs. 4a to 4d, and $\epsilon_B \equiv \epsilon$ in Figs. 4a to 4d.

Thus the procedure for the evaluation of the downwash at a given tailplane position, h/c and l/c, and given α, C_J and τ, is to calculate the functions in the following order:

(i) X from equation (8*a*)

(ii) z_J from Fig. 3

(iii) Z from equation (8*b*)

(iv) $\partial\epsilon/\partial\tau$, $\partial\epsilon/\partial\alpha$ from Figs. 4a to 4d

(v) ϵ from equation (11).

Interpolation will be necessary for C_J values other than 0·5, 1·0, 2·0 and 4·0, and it seems better to evaluate ϵ for a range of C_J, and then to interpolate the final result, rather than to interpolate for z_J, $\partial\epsilon/\partial\tau$ and $\partial\epsilon/\partial\alpha$ separately.

For large X, the downwash is given by

$$\epsilon(X, o) \simeq \frac{A_0\tau + (B_0 + \frac{1}{2})\alpha}{X} = \frac{C_L}{4\pi X}, \qquad (see \text{ Ref. 1})$$

so that

$$\left.\begin{aligned} \frac{\partial\epsilon}{\partial\tau} &\simeq \frac{A_0}{X} = \frac{\left(\frac{\partial C_L}{\partial\tau}\right)}{4\pi X} \\ \text{and} \\ \frac{\partial\epsilon}{\partial\alpha} &\simeq \frac{(B_0 + \frac{1}{2})}{X} = \frac{\left(\frac{\partial C_L}{\partial\alpha}\right)}{4\pi X} \end{aligned}\right\} \text{ as } X \to \infty .$$

It may be noted that the value of $C_L/(4\pi X)$ for the downwash far behind the aerofoil is also obtained when the aerofoil is without a jet-flap.

3. *Results.* The results for the downwash behind an infinite wing and jet-flap are shown in Figs. 7 to 11. It should be remembered that the theory is only strictly valid for small α and τ, so that the use of the method to obtain the downwash for the larger values of α and τ must wait to be justified or otherwise until experimental data are available. However, the results should indicate the trends in the variation of downwash with the various parameters.

In Figs. 7 and 8, the variation of the downwash with tailplane position is shown for two values of jet deflection angle, τ, and two values of wing incidence, α, for $C_J = 2{\cdot}0$. Fig. 7 shows that on the extended chord-line, $h/c = 0$, the downwash decreases quite sharply with increasing distance behind the wing, l/c, but when $h = 2c$, the downwash is practically constant in each case for $3c < l < 5c$. The results have been replotted in Fig. 8 to show the downwash field (*i.e.*, contours of equal downwash), in the tailplane region. A comparison between the fields for the various τ and α shows that the downwash is more sensitive to tailplane position for the higher τ and α values, as might be expected.

The results for the variation of ϵ with C_J, τ and α are given in Figs. 9 and 10 for a representative tailplane position, $l/c = 3{\cdot}5$, $h/c = 1{\cdot}5$, and also for a position on the extended chord-line, $l/c = 3{\cdot}5$, $h/c = 0$. It will be noticed in Fig. 9a that ϵ does not increase linearly with τ for a given C_J value (as might be implied by a glance at equation (11)) due to the correction made to the downwash field for the displacement of the jet relative to the tailplane position. Fig. 9b indicates that $\partial\epsilon/\partial C_J$ decreases with increasing C_J. The variation of downwash with wing incidence is more

important for stability and control considerations and the results are shown in Figs. 10a to 10d for $\tau = 30$ and 60 deg, and for various C_J values. Ranges of values of $(\partial\epsilon/\partial\alpha)_{\alpha=0}$ are also indicated on the diagrams, and are seen to be the same for the two different τ values over the same range of C_J for a given value of h/c. Since $(\partial\epsilon/\partial\alpha)_{\alpha=0}$ increases with C_J, it is not possible to assess a maximum, but for $C_J = 4{\cdot}0$, $(\partial\epsilon/\partial\alpha)_{\alpha=0}$ is well below $1{\cdot}0$ at the tailplane and on the extended chord-line, being $0{\cdot}20$ and $0{\cdot}35$ respectively. It also appears that $\partial\epsilon/\partial\alpha$ increases as α increases, but this is only noticeable at the higher values of C_J, and for $C_J = 4{\cdot}0$, $\alpha = 20$ deg, $\partial\epsilon/\partial\alpha$ is still less than $0{\cdot}4$ at the extended chord-line position.

The dependence of the downwash on the lift coefficient is shown in Fig. 11 as the variation of ϵ/C_L with C_L, again for the two values of $h = 0$ and $1{\cdot}5c$ at $l = 3{\cdot}5c$. For a plain wing, ϵ/C_L is a constant for a given tailplane position, but Fig. 11 shows that this is not so for a wing with a jet-flap. The series of 'carpets' which appear on a complete ϵ/C_L vs. C_L diagram (α, C_J and τ varying), have been separated into the special cases of $\alpha = 0$ deg, $C_J = 2{\cdot}0$ and $\tau = 30$ deg in turn, each with the other two parameters varying, e.g., for $C_J = 2{\cdot}0$, the curves for $\alpha = 0$ deg and $\alpha = 10$ deg with varying τ and those for $\tau = 30$ deg and $\tau = 60$ deg with varying α are shown, so that one carpet appears. The curves are labelled with the value of the constant parameter on the right-hand side, and the varying parameter on the left-hand side. For $h/c = 0$, it is seen that the majority of values of ϵ/C_L lie between $1{\cdot}2$ and $1{\cdot}6$ deg in the C_L range $1{\cdot}0$ to $8{\cdot}0$, and for $h/c = 1{\cdot}5$, the limits are approximately $0{\cdot}7$ and $1{\cdot}1$ deg. It may be mentioned that in an investigation of stability and control characteristics of jet-flapped aircraft, based on two-dimensional data, Taylor[4] used a constant value for ϵ/C_L of $0{\cdot}025$ radn $= 1{\cdot}4$ deg, which is of the correct order for small values of h/c. It is interesting to note that for $C_J = 2{\cdot}0$, ϵ/C_L increases with C_L if τ is constant and α is increasing, but decreases as C_L increases if α is constant and τ is increasing.

The values of ϵ/C_L for an infinite wing without a jet-flap, obtained by representing the wing by a vortex at the quarter-chord point, are $1{\cdot}40$ deg for $h = 0$ and $1{\cdot}16$ deg for $h = 1{\cdot}5c$, the former being a good approximation when compared with Fig. 11, but the latter value is appreciably greater than those obtained by the present theory, where the average value of ϵ/C_L is $0{\cdot}9$ deg. For large X, the value of ϵ/C_L given by this approximate method is $1/(4\pi X)$, i.e., it converges to the same value as given above in Section 2.

PART II

1. *Vortex Representation of the Wing and Jet-Flap of Finite Span.* As for the wing of infinite span, the pressure (and so velocity) difference across the wing and jet surfaces may be represented by sheets of spanwise bound vorticity, but for the finite wing there is also a pressure gradient along the span, which gives rise to streamwise trailing vorticity on the wing and jet surfaces.

Maskell[2] has shown that the distribution of bound vorticity on a chordwise section of the finite wing and jet is approximately that on a two-dimensional wing and jet at an effective aerofoil incidence (α_e) and effective jet momentum coefficient $C_{J\,e}$. Thus the contribution to the downwash from the bound vorticity may be evaluated as in Part I, using $C_{J\,e}$ and α_e in place of C_J and α, but in this case the resulting downwash field must be displaced through the total jet displacement, *i.e.*, the sum of the displacements due to the trailing vortices and to the bound vortices respectively. In order to evaluate the downwash and displacement induced by the trailing vortices, the assumption is made that the loading is concentrated on and near to the wing, so that the trailing vortices arise

from one chordwise position, taken to be the centre of pressure of the effective infinite wing. Since the loading is also assumed to be elliptic, the induced downwash may be evaluated in the usual way[3].

The representation of the finite wing is shown in Fig. 2. Let the origin of the non-dimensional co-ordinates x, y, z (based on the chord being unity), be taken at the mid-span of the leading edge, and let $U_0F(x)$ be the bound vorticity distribution on a section of the wing and jet. Then Maskell[2] has shown that $U_0F(x)$ is approximately the vorticity distribution on a wing and jet of infinite span at wing incidence α_e, jet momentum coefficient $C_{J\,e}$ and jet deflection τ, where

$$\frac{C_{J\,e}}{C_J} = 1 - \frac{\alpha_i}{\tau + \alpha_e}, \tag{12}$$

$$\alpha_i = \alpha - \alpha_e$$

$$= \frac{C_L}{\pi A + 2C_J}, \tag{13}$$

C_L being the lift on the finite wing.

Also

$$C_L = a_{0e}\,\tau + a_{1e}\alpha_e + 2C_J\alpha_i, \tag{14}$$

where a_{0e} and a_{1e} are functions of $C_{J\,e}$ only, whose values are given in Table 1, for $C_{J\,e} = 0{\cdot}5$, $1{\cdot}0$, $2{\cdot}0$ and $4{\cdot}0$. Hence

$$\left.\begin{aligned} \alpha_i &= \frac{a_{0e}\tau + a_{1e}\alpha}{\pi A + a_{1e}} \\ \text{and} \qquad \alpha_e &= \frac{\pi A\alpha - a_{0e}\tau}{\pi A + a_{1e}} \end{aligned}\right\} \tag{15}$$

These values of $C_{J\,e}$, α_e and τ may be used in Spence's solution to give $U_0F(x)$ and the displacement of the wake due to the bound vortices from equations (1) to (5), with α and C_J replaced by α_e and $C_{J\,e}$ respectively.

The trailing vortices are assumed to arise from a lifting line at the centre of pressure of the effective wing, *i.e.*, at

$$x = x_p = \left(\frac{C_m}{C_L}\right)_e = \frac{b_{0e}\tau + b_{1e}\alpha_e}{a_{0e}\tau + a_{1e}\alpha_e}, \tag{16}$$

where b_{0e} and b_{1e} are functions of $C_{J\,e}$ only, whose values are also given in Table 1 for $C_{J\,e} = 0{\cdot}5$, $1{\cdot}0$, $2{\cdot}0$ and $4{\cdot}0$. For elliptic loading, the strength of the trailing vortices is

$$-U_0\frac{d\Gamma}{dy},$$

where

$$\Gamma = \frac{4sC_L}{\pi A}\sin\theta, \qquad y = -s\cos\theta, \tag{17}$$

and s is the semi-span of the wing, based on the chord being unity.

---

* This relation assumes that $\alpha_i = \frac{1}{2}\alpha_\infty$, which is not strictly true for large C_J values, but the approximation is acceptable in this context.

2. *The Downwash due to the Bound Vorticity.* The downwash at the point (X, Y, Z) due to the bound vorticity on a finite wing and jet of span $b = 2s$, with elliptic loading and $U_0F(x)$ as the bound vorticity distribution at the mid-span, is

$$w_B(X, Y, Z) = \frac{1}{4\pi}\int_{y=-s}^{+s}\int_{x=0}^{\infty}\frac{U_0F(x)\left\{1-\left(\frac{y}{s}\right)^2\right\}^{1/2}(X-x)}{\{(X-x)^2+(Y-y)^2+Z^2\}^{3/2}}\,dx\,dy \tag{18}$$

to the first order in α and τ.

In the plane of symmetry, $Y = 0$, the downwash becomes

$$w_B(X,O,Z) = \frac{1}{4\pi}\int_{x=0}^{\infty}U_0F(x)(X-x)\int_0^{\pi}\frac{\sin\theta\, s\sin\theta\, d\theta}{\{(X-x)^2+s^2\cos^2\theta+Z^2\}^{3/2}}\,dx\,,$$

where $y = -s\cos\theta$, i.e.,

$$w_B(X,O,Z) = \frac{1}{4\pi}\int_{x=0}^{\infty}\frac{U_0F(x)(X-x)}{\{(X-x)^2+s^2+Z^2\}^{3/2}}\,2\int_0^{\pi/2}\frac{s\sin^2\theta\, d\theta}{\left[1-\frac{s^2\sin^2\theta}{\{(X-x)^2+s^2+Z^2\}}\right]^{3/2}}\,dx\,.$$

Let

$$k^2 = \frac{s^2}{(X-x)^2+s^2+Z^2}\,,$$

so that

$$k'^2 = 1-k^2 = \frac{(X-x)^2+Z^2}{(X-x)^2+s^2+Z^2}\,.$$

Then

$$w_B(X,O,Z) = \frac{1}{2\pi}\int_{x=0}^{\infty}\frac{U_0F(x)(X-x)}{\{(X-x)^2+Z^2\}}\,k'^2\int_0^{\pi/2}\frac{k\sin^2\theta\, d\theta}{(1-k^2\sin^2\theta)^{3/2}}\,dx$$

$$= \frac{1}{2\pi}\int_{x=0}^{\infty}\frac{U_0F(x)(X-x)}{\{(X-x)^2+Z^2\}}\,\frac{1}{k}\,(E_1-k'^2K_1)\,dx\,, \tag{19}$$

where K_1 and E_1 are the complete elliptic integrals of the first and second kinds respectively, and equation (19) has been derived using Art. 74 of *Cayley's Elliptic Functions* (Cambridge University Press, 2nd Edition, 1895).

Within the range (O,∞) of the variable x, the function $(1/k)\,(E_1 - k'^2K_1)$ is found to have a maximum value of approximately 1 at $x = X$, and values of approximately $0\cdot5$ at $x = 0$ and $x = 2X$. Furthermore, it tends to zero as x tends to infinity. Thus for the range of x for which the function

$$\frac{F(x)(X-x)}{(X-x)^2+Z^2}$$

has values differing significantly from zero and over which the major contribution to the integral (19) occurs, that is, the range $0 < x < 2X$*, the function $(1/k)\,(E_1 - k'^2K_1)$ is of the order 1, and so the approximation is made that it is equal to 1 throughout the range of integration. It would,

---

* The fact that the remaining part of the range of integration is infinite does not invalidate this argument, since for the numerical evaluation the part of the integral (19) over the range $(1,\infty)$ of x is transformed into an integral over a finite range (O,π) of ϕ, say. The integrand is then $\frac{F(x)(X-x)}{(X-x)^2+Z^2}\frac{dx}{d\phi}$, which is still small in the range of ϕ corresponding to $x > 2X$.

perhaps, be more logical to adopt a value somewhat less than 1·0, but in view of the fact that the downwash due to the trailing vorticity is found to be much greater than that due to the bound vorticity, the approximation $(1/k)(E_1 - k'^2K_1) = 1$ is considered acceptable. The error in the total downwash arising from this approximation is estimated to be less than 12 per cent for large-aspect-ratio wings ($A = 6$, say).

Thus equation (19) becomes

$$w_B(X,O,Z) = \frac{1}{2\pi}\int_{x=0}^{\infty} \frac{U_0F(x)(X-x)}{(X-x)^2 + Z^2}\,dx\,, \tag{20}$$

where

$$U_0F(x) = U_0f(x) \text{ on the wing,} \qquad 0 < x < 1$$
$$U_0F(x) = \gamma(x) \qquad \text{on the jet,} \qquad 1 < x < \infty$$

and $f(x)$ and $\gamma(x)$ are given by equations (2) and (5) with $C_J \equiv C_{Je}$ and $\alpha \equiv \alpha_e$, i.e., $w_B(X,O,Z)$ is the downwash due to the effective infinite wing, and may be evaluated as in Part I.

3. *The Downwash due to the Trailing Vorticity.* The downwash at the point (X,Y,Z) due to the trailing vorticity of strength $U_0(d\Gamma/dy)$ lying in the plane $z = 0$ is

$$w_T(X,Y,Z) = -\frac{1}{4\pi}\int_{y=-s}^{+s}\int_{x=x_p}^{\infty} U_0\frac{d\Gamma}{dy}\frac{(y-Y)}{\{(x-X)^2 + (y-Y)^2 + Z^2\}^{3/2}}\,dx\,dy$$
$$= -\frac{1}{4\pi}\int_{y=-s}^{+s} U_0\frac{d\Gamma}{dy}\frac{(y-Y)}{\{(y-Y)^2+Z^2\}}\left[1 - \frac{x_p - X}{\{(x_p-X)^2 + (y-Y)^2 + Z^2\}^{1/2}}\right]dy$$

where x_p is given in equation (16).

From equation (17) we have that

$$U_0\frac{d\Gamma}{dy} = U_0\frac{4sC_L}{\pi A}\frac{\cos\theta}{s\sin\theta}\,,$$

and so

$$w_T(X,Y,Z) = -\frac{4sC_L}{4\pi^2 A}U_0\int_0^{\pi}\frac{\cos\theta}{s\sin\theta}\frac{(-s\cos\theta - Y)}{\{(-s\cos\theta - Y)^2 + Z^2\}} \times$$
$$\left[1 + \frac{X - x_p}{\{(X-x_p)^2 + Z^2 + (s\cos\theta + Y)^2\}^{1/2}}\right] s\sin\theta\,d\theta$$
$$= \frac{sC_L}{A\pi^2}U_0\int_0^{\pi}\frac{\cos\theta\,(s\cos\theta + Y)}{\{(s\cos\theta + Y)^2 + Z^2\}}\left[1 + \frac{X - x_p}{\{(X-x_p)^2 + Z^2 + (s\cos\theta + Y)^2\}^{1/2}}\right]d\theta\,.$$

In the plane of symmetry $Y = 0$, the downwash angle due to the trailing vorticity thus becomes

$$\epsilon_T = \frac{w_T(X,O,Z)}{U_0}$$
$$= \frac{2C_L}{\pi A}\frac{1}{2\pi}\int_0^{\pi}\frac{\cos^2\theta}{\left\{\cos^2\theta + \left(\frac{Z}{s}\right)^2\right\}}\left[1 + \frac{\left(\frac{X-x_p}{s}\right)}{\left\{\cos^2\theta + \left(\frac{X-x_p}{s}\right)^2 + \left(\frac{Z}{s}\right)^2\right\}^{1/2}}\right]d\theta$$
$$= \frac{2C_L}{\pi A}I(\xi,\zeta)\,, \tag{21}$$

where

$$\xi = \frac{X - x_p}{s}, \qquad \zeta = \frac{Z}{s} \tag{22}$$

and

$$I(\xi,\zeta) = \frac{1}{2\pi}\int_0^\pi \frac{\cos^2\theta}{(\cos^2\theta + \zeta^2)}\left\{1 + \frac{\xi}{(\cos^2\theta + \xi^2 + \zeta^2)^{1/2}}\right\} d\theta$$

$$= \frac{1}{2\pi}\int_0^\pi \left\{1 - \frac{\zeta^2}{(1 + \zeta^2 - \sin^2\theta)}\right\}\left\{1 + \frac{\xi}{(1 + \xi^2 + \zeta^2 - \sin^2\theta)^{1/2}}\right\} d\theta .$$

Let

$$n = -\frac{1}{1 + \zeta^2} \quad \text{and} \quad k^2 = \frac{1}{1 + \xi^2 + \zeta^2}, \tag{23}$$

then

$$I(\xi,\zeta) = \frac{1}{2\pi}\int_0^\pi \left\{1 + \frac{\zeta^2 n}{1 + n\sin^2\theta} + \frac{\xi k}{(1 - k^2\sin^2\theta)^{1/2}} + \frac{\zeta^2\xi n k}{(1 + n\sin^2\theta)(1 - k^2\sin^2\theta)^{1/2}}\right\} d\theta$$

$$= \frac{1}{2\pi}\left\{\pi + \frac{\zeta^2 n}{\sqrt{(1+n)}}\pi + 2\xi k K_1(k) + 2\zeta^2\xi n k \Pi_1(k,n)\right\}$$

$$= \frac{1}{2}\left\{1 - \frac{\zeta}{(1 + \zeta^2)^{1/2}} + \frac{2}{\pi}\frac{\xi}{(1 + \xi^2 + \zeta^2)^{1/2}} K_1(k) - \frac{2}{\pi}\frac{\zeta^2\xi}{(1 + \zeta^2)(1 + \xi^2 + \zeta^2)^{1/2}}\Pi_1(k,n)\right\}, \tag{24}$$

where $\Pi_1(k,n)$ is the complete elliptic integral of the third kind. A chart is given in Fig. 6 for the function $I(\xi,\zeta)$, so that ϵ_T may be evaluated from equation (21).

4. *The Displacement of the Jet and Trailing Vortices.* As in the case of the wing of infinite span, the displacement of the wake due to the bound vortices may be obtained from Fig. 3, using the relationship

$$z_J(X) = \left(\frac{\partial z_J}{\partial \tau}\right)_e \tau + \left(\frac{\partial z_J}{\partial \alpha}\right)_e \alpha_e . \tag{25}$$

The contribution due to the trailing vortices may be derived from the induced downwash at the wake, since

$$w_i = U_0 \frac{dz_i}{dx}, \tag{26}$$

where

w_i = induced downwash at the wake

z_i = induced displacement of the wake.

The value of w_i is given by equations (21) and (24) when $X = x$, $Y = 0$, $Z = 0$, i.e., $\xi = (x - x_p)/s$, $\zeta = 0$. Thus

$$w_i(x) = U_0 \frac{2C_L}{\pi A}\frac{1}{2}\left\{1 + \frac{2\xi}{\pi(1 + \xi^2)^{1/2}} K_1(k_0)\right\},$$

where

$$k_0^2 = \frac{1}{1 + \xi^2},$$

and so

$$z_i(x) = \frac{C_L}{\pi A}\int_{x_p}^{x}\left\{1 + \frac{2}{\pi}(1 - k_0^2)^{1/2}K_1(k_0)\right\}dx$$

$$= \frac{C_L}{\pi A}\left\{x - x_p + \frac{2}{\pi}\int_1^{k_0}(1 - k_0^2)^{1/2}K_1(k_0)\frac{dx}{dk_0}\,dk_0\right\}. \qquad (27)$$

Now

$$\xi^2 = \left(\frac{x - x_p}{s}\right)^2 = \frac{1 - k_0^2}{k_0^2},$$

giving that

$$\frac{2}{\pi}\int_1^{k_0}(1 - k_0^2)^{1/2}\,K_1(k_0)\frac{dx}{dk_0}\,dk_0 = -\frac{2}{\pi}\int_1^{k_0}(1 - k_0^2)^{1/2}\,K_1(k_0)\frac{s}{k_0^2\,(1 - k_0^2)^{1/2}}\,dk_0$$

$$= -\frac{2s}{\pi}\int_1^{k_0}\frac{K_1(k_0)}{k_0^2}\,dk_0$$

$$= -\frac{2s}{\pi}\int_{\bar{1}}^{k}\int_0^{\pi/2}\frac{d\theta\,dk_0}{k_0^2(1 - k_0^2\sin^2\theta)^{1/2}}$$

$$= -\frac{2s}{\pi}\int_0^{\pi/2}\int_{\cos\theta}^{t}\frac{\sin\theta\,(-\,t\,dt)}{(1 - t^2)^{3/2}\,t}\,d\theta,$$

where $t^2 = 1 - k_0^2\sin^2\theta$

$$= -\frac{2s}{\pi}\int_0^{\pi/2}\sin\theta\left\{-\frac{(1 - k_0^2\sin^2\theta)^{1/2}}{k_0\sin\theta} + \frac{\cos\theta}{\sin\theta}\right\}d\theta$$

$$= -\frac{2s}{\pi}\left[-\frac{E_1(k_0)}{k_0} + 1\right]$$

and so equation (27) becomes

$$z_i(x) = \frac{C_L b}{2\pi A}\left\{\frac{x - x_p}{s} + \frac{2}{\pi}\frac{E_1(k_0)}{k_0} - \frac{2}{\pi}\right\}. \qquad (28)$$

The function $\{z_i(X)/C_L\}(A/b)$ is shown in Fig. 5, as a function of $\xi = (X - x_p)/s$.

The complete downwash field $w_B(X,O,Z) + w_T(X,O,Z)$ obtained from equations (20) and (21) must now be displaced through a distance $z_J(X) + z_i(X)$, so that the wake is in the correct position relative to the tailplane, *i.e.*, downwash at $(X,O,Z + z_J(X) + z_i(X))$

$$= w_B(X,O,Z) + w_T(X,O,Z). \qquad (29)$$

As for the wing of infinite span, the position of the tailplane is given in terms of l, the distance behind the wing leading edge, and h, the height above the extended chord-line, and so for the evaluation of the downwash at the tailplane,

$$X = \frac{l}{c} + \frac{h}{c}\alpha, \qquad (30a)$$

$$Z = -H = \frac{l}{c}\alpha - \frac{h}{c} - z_J(X) - z_i(X). \qquad (30b)$$

The functions required in the analysis may be evaluated in the following order for given A, h/c, l/c, α, τ and effective jet momentum coefficient C_{Je}.:

(i) α_e from equation (15) using Table 1

(ii) C_J from equation (12)

(iii) C_L from equation (13)

(iv) x_p from equation (16) using Table 1

(v) X from equation (30*a*)

(vi) ξ from equation (22)

(vii) $z_J(X)$ from Fig. 3

(viii) $z_i(\xi)$ from Fig. 5

(ix) Z from equation (30*b*)

(x) ζ from equation (22)

(xi) $I(\xi,\zeta)$ from Fig. 6

(xii) ϵ_T from equation (21)

(xiii) $\partial\epsilon_B/\partial\tau$, $\partial\epsilon_B/\partial\alpha$ from Fig. 4

(xiv) ϵ_B from equation (11)

giving $\epsilon = \epsilon_B + \epsilon_T$.

It seems simpler to work in terms of the C_{Je} as indicated above, and then to interpolate for a required C_J, as it is quicker to work through the procedure for three C_{Je} values for which $\partial z_J/\partial\tau$, etc., are shown graphically, in order to find the variation of ϵ with C_J, than to work through once with the C_{Je} corresponding to the given C_J, having to interpolate at each step.

For large X, it is possible to obtain a good approximation to the downwash far behind the wing without a jet-flap, by using the relation

$$\epsilon(X,O,O) = \frac{2C_L}{\pi A}\left(1 + \frac{s^2}{\pi^2 X^2}\right). \tag{31}$$

However, in the present case of a wing with a jet-flap, the downwash far downstream is affected by the bound vortices in the wake, and these contribute a term $[(C_L A)/\{4(\pi A + 2C_J)\}](1/X)$, the next terms in the series being of order $1/X^{3/2}$ and $1/X^2$ with coefficients which are complicated functions of the Fourier-series coefficients $A_0 \ldots A_n$ and $B_0 \ldots B_n$. Thus the approximation to the downwash for large X, if taken to the same degree of accuracy as that in equation (31), is too unwieldy to be useful.

5. *Results.* A few American experimental results for the downwash behind a jet-flapped wing of aspect ratio 8·4 were available, at the time of writing, and these are compared with the theoretical results in Fig. 12. More general results, calculated for a wing of aspect ratio 6·0, are given in Figs. 13 to 17.

In the American experiments, the wing was tested at zero incidence with $C_J = 1{\cdot}6$ and $\tau = 60$ deg, and it is seen in Fig. 12 that the experimental downwash is greater than the theoretical values at the same tailplane positions. However, the experimental lift coefficient is given as 5·2, whereas

the theoretical value given by equations (12) to (15) is 4·2*, and so the calculations were repeated using the experimental value of C_L. The results obtained in this way are also shown in Fig. 12, and are seen to agree very well with the experimental curves.

The theoretical results for the downwash on the centre-line for the aspect-ratio-6 wing are presented in Figs. 13 to 17 in a way similar to that used for the infinite wing. The variation of downwash with tailplane position, Fig. 13, is given for the cases $C_{J_e} = 2{\cdot}0$ ($C_J = 2{\cdot}7$ to $3{\cdot}0$), $\tau = 30$ and 60 deg, $\alpha = 0$ and 10 deg. As for the infinite wing, the downwash varies only slightly with the distance behind the wing when $h = 2c$. The corresponding downwash fields in the neighbourhood of the tailplane are shown in Fig. 14.

The variation of the downwash with the wing and jet parameters is again considered for the tailplane positions $l = 3{\cdot}5c$, $h = 1{\cdot}5c$, and on the extended chordline at $l = 3{\cdot}5c$, $h = 0$. Fig. 15 shows the effect of varying the jet parameters, and it may be seen that the downwash at the tailplane is about half that on the extended chord-line. The values of $(\partial\epsilon/\partial\alpha)_{\alpha=0}$ derived from Figs. 16a to 16d are found to be appreciably larger than those obtained in Fig. 10 for the infinite wing, being approximately constant at $0{\cdot}70$ for $h = 0$ and $0{\cdot}35$ for $h = 1{\cdot}5c$ for the various C_J values when $\tau = 30$ deg, and varying between $0{\cdot}40$ and $0{\cdot}60$ for $h = 0$ and between $0{\cdot}15$ and $0{\cdot}30$ for $h = 1{\cdot}5c$ when $\tau = 60$ deg. Thus $\partial\epsilon/\partial\alpha$ decreases with increasing τ, and also with increasing α and C_J, as the graphs show, although ϵ itself increases. However, even for the lowest values of α, C_J and τ considered ($\alpha = -10$ deg, $C_J = 0{\cdot}5$, $\tau = 30$ deg), $\partial\epsilon/\partial\alpha$ is still well below $1{\cdot}0$ at the tailplane position.

The carpet plots of ϵ/C_L against C_L (Fig. 17), are similar in shape to those for the infinite wing (Fig. 11), but the values of ϵ/C_L are much greater, being between 3 and $6{\cdot}5$ deg for $h = 0$ or between $1{\cdot}5$ and $3{\cdot}5$ deg for $h = 1{\cdot}5c$, in the C_L range 1 to 8, as compared with the ranges $1{\cdot}2$ to $1{\cdot}6$ deg for $h = 0$ or $0{\cdot}7$ to $1{\cdot}1$ deg for $h = 1{\cdot}5c$ obtained from Fig. 11. The carpet plots of ϵ/C_L for a wing without a jet-flap are also shown in Fig. 17, the lift being equal to that on the jet-flapped wing in each case, and the values of ϵ/C_L being obtained from the Data Sheets: Aircraft 08.01.04 and 08.01.02 of the Royal Aeronautical Society. It is seen that the data sheets underestimate ϵ/C_L for the position on the extended-wing chord-line, but at the tailplane height of $1{\cdot}5c$, the agreement is good for some specific combinations of values of C_J, τ and α, e.g., $C_J = 2{\cdot}0$, $\alpha = 10$ deg, $\tau = 30$ and 60 deg. However, it does not seem possible to estimate the possible error in using the results from the data sheets for a given C_L, because the parameters C_J, τ and α affect the downwash and lift coefficient in different ways.

Conclusions. The downwash behind jet-flapped wings has been evaluated, using the thin-aerofoil theories given by Spence[1] and Maskell[2], for wings of infinite and finite span respectively, to obtain the strength and position of the vortex sheets which represent the wing and the jet. Thus the basic assumptions are that the wing incidence and jet deflection are small, and that the finite wing is elliptically loaded. It is also assumed that the trailing vorticity on the finite wing may be represented by a vortex sheet arising from one chordwise position on the wing. The resulting downwash fields have then been displaced so that the jet is in the correct position relative to the tailplane.

---

* This difference is mainly due to the use of a blown flap on the experimental model, rather than a jet-flap. The downwash will also be different, and for the blown flap it could be calculated using the results of Ref. 7 in place of Ref. 1, i.e., $\partial z_J/\partial\tau$, $\partial\epsilon_B/\partial\tau$, a_{0e} and b_{0e} must be changed. However, for the present comparison, it is sufficient to take the difference as being due only to the increase in lift.

The agreement with the few experimental results available is quite good, especially if the experimental C_L value (which is appreciably greater than the theoretical value*), is used in the calculations. The variations of the downwash with tailplane position, wing incidence and jet parameters follow similar patterns for the infinite and finite wings, although the effect of reducing the aspect ratio from infinity to 6·0 is to increase the downwash by factors ranging between 2 and 4 for the configurations considered. Of the derivatives with respect to the wing and jet parameters, $\partial\epsilon/\partial\alpha$ is the most important from the point of view of aircraft stability, and it appears to be well below the critical value of 1·0 for tailplane positions above the extended-wing chord-line. One major difference between the infinite and finite wings is noticeable here, in that $\partial\epsilon/\partial\alpha$ increases with increasing α and C_J, and is nearly constant with increasing τ for the infinite wing, but it decreases as α, C_J and τ increase for the wing of aspect ratio 6·0. It is found that ϵ/C_L is not a constant for a given tailplane position, when considered as a function of C_L, due to the fact that there are three parameters (α, C_J and τ) which may be varied to obtain any given C_L, and these affect the downwash in different ways.

No consideration has been given in this report to the effect of the rolling-up of the vortex sheets in the wake when the aspect ratio is finite, but some rough calculations have been made based on a completely rolled-up trailing vortex system, and those indicate that the downwash on the centre-line will be increased somewhat at tailplane positions near the jet when rolling-up takes place.

---

* The theoretical value for a blown flap is also greater than that for a jet-flap, for the same angle of incidence of the main wing.

LIST OF SYMBOLS

Note. 'Infinite' refers to the infinite-span wing in Part I and to the effective infinite wing in Part II when the symbol occurs in both Part I and Part II.

a_{0e}		$\partial C_L/\partial\tau$ for effective infinite wing
a_{1e}		$\partial C_L/\partial\alpha$ for effective infinite wing
b_{0e}		$\partial C_m/\partial\tau$ for effective infinite wing
b_{1e}		$\partial C_m/\partial\alpha$ for effective infinite wing
A		Aspect ratio
A_n, B_n		Fourier-series coefficients
b		Wing span, based on the chord being unity
c		Wing chord
C_J		Jet momentum coefficient
C_{Je}		Effective jet momentum coefficient
C_L		Lift coefficient
$E_1(k)$		Complete elliptic integral of the second kind
$f(x)$	$=$	$f_1\tau + f_2\alpha$ (Non-dimensional vorticity on infinite wing)
$F(x)$		Non-dimensional bound vorticity on finite wing and jet
h		Height of tailplane $\frac{1}{4}$-chord point above the extended wing chord-line
$I(\xi, \zeta)$		Function introduced in equation (21)
k, k_0, n		Variables for the elliptic integrals
$K_1(k)$		Complete elliptic integral of the first kind
l		Distance of tailplane $\frac{1}{4}$-chord point behind the wing leading edge
s		Wing semi-span, based on the chord being unity
U_0		Mainstream velocity
w_B		Downwash velocity due to bound vorticity on effective wing and jet
w_T		Downwash velocity due to trailing vorticity
w_i		Induced velocity due to trailing vorticity at the wake
w		Complete downwash at the tailplane
(x,y,z)		Non-dimensional co-ordinates, based on the chord of the wing being unity
x_p		Distance of centre of pressure of effective infinite wing behind wing leading edge
z_J		Displacement of infinite jet
z_i		Induced displacement of the trailing vortex sheet
$(\bar{X}, Y, Z)$		Co-ordinates of point at which downwash is to be evaluated
α		Incidence of wing

LIST OF SYMBOLS—*continued*

α_e		Effective incidence of wing
$\gamma(x)$	=	$U_0(\gamma_1\tau + \gamma_2\alpha)$ Vorticity on infinite jet
$U_0\Gamma(y)$		Total bound vorticity on wing and jet at any spanwise station
$\epsilon = w/U_0$		Angle of downwash, with corresponding subscripts B, T, as for the downwash velocity
Π_1		Complete elliptic integral of third kind
τ		Angle of ejection of the jet relative to wing chord
ξ, ζ		'Co-ordinates' introduced in equation (22)

REFERENCES

No.	Author	Title, etc.
1	D. A. Spence	A treatment of the jet-flap by thin aerofoil theory. *Proc. Roy. Soc.* (*A*). Vol. 238. pp. 46 to 48. 1956.
2	E. C. Maskell and D. A. Spence ..	A theory of the jet-flap in three-dimensions. R.A.E. Report (To be published.)
3	H. Multhopp	The calculation of downwash behind wings. *L.F.F.* Vol. 15. 1938.
4	A. S. Taylor	An examination of some longitudinal stability and control problems of jet-flap aircraft with particular reference to the use of jet thrust and jet-flap deflection controls. R.A.E. Report (To be published.)
5	R. D. Vogler and T. R. Turner	Wind-tunnel investigation at low speeds to determine flow-field characteristics and ground interference on a model with jet-augmented flaps. N.A.C.A. Tech. Note 4116. September, 1957.
6	J. R. Spreiter and A. H. Sacks	The rolling-up of the trailing vortex sheet and its effect on the downwash behind wings. *J.Ae.Sci.* Vol. 18. No. 1. 1951.
7	D. A. Spence	The lift on a thin aerofoil with a jet-augmented flap. *Aero. Quart.* Vol. IX. August, 1958.

TABLE 1

$C_{J\,e}$	$a_{0e} = \left(\frac{\partial C_L}{\partial \tau}\right)_e$	$a_{1e} = \left(\frac{\partial C_L}{\partial \alpha}\right)_e$	$b_{0e} = \left(\frac{\partial C_m}{\partial \tau}\right)_e$	$b_{1e} = \left(\frac{\partial C_m}{\partial \alpha}\right)_e$
0·5	2·707	7·588	1·485	1·898
1·0	4·026	8·605	2·315	2·097
2·0	6·135	10·405	3·745	2·396
4·0	9·638	13·609	6·307	2·836

(78824)

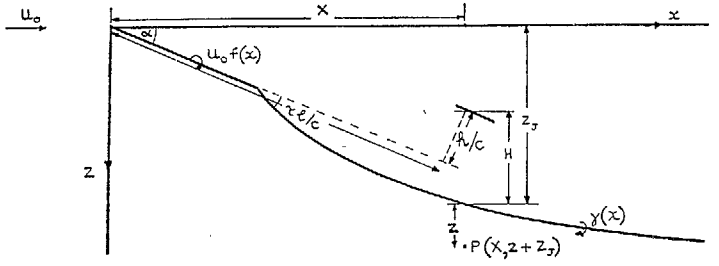

FIG. 1a. Section of infinite-span wing, showing jet and tailplane positions.

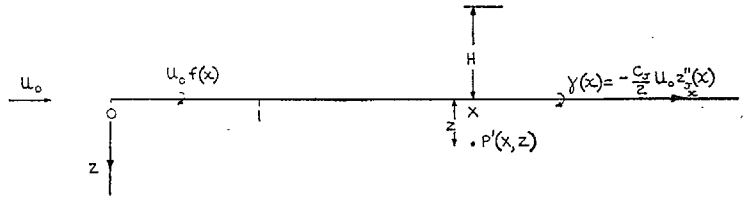

FIG. 1b. Vorticity distributions and tailplane position as used in calculations.

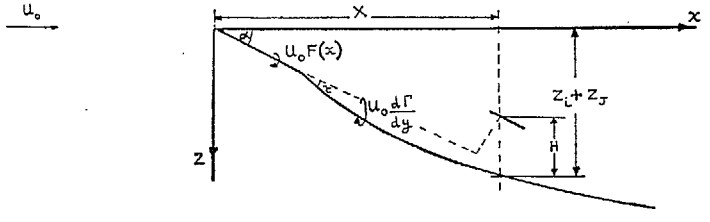

FIG. 2a. Section of finite-span wing, showing jet and tailplane position.

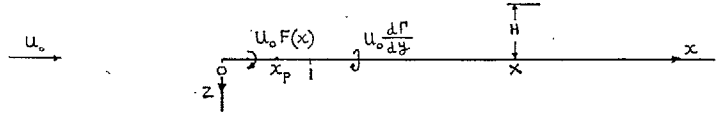

FIG. 2b. Vorticity distributions and tailplane position on centre-line of wing.

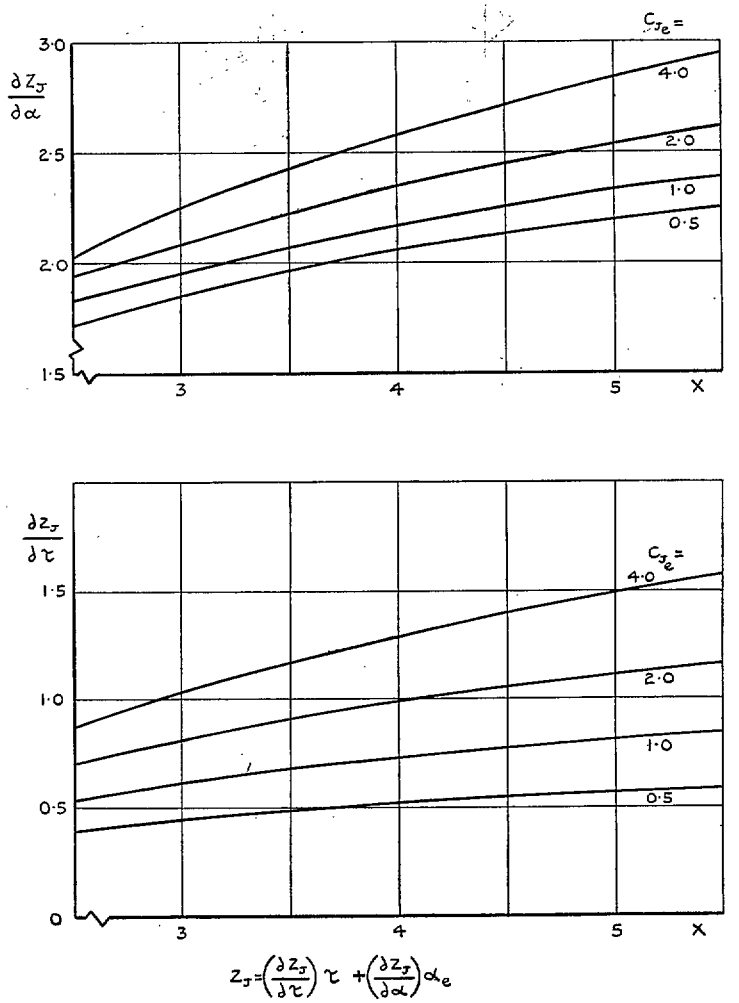

FIG. 3. Charts for determination of jet displacement (infinite wing), or jet displacement due to bound vorticity (finite wing).

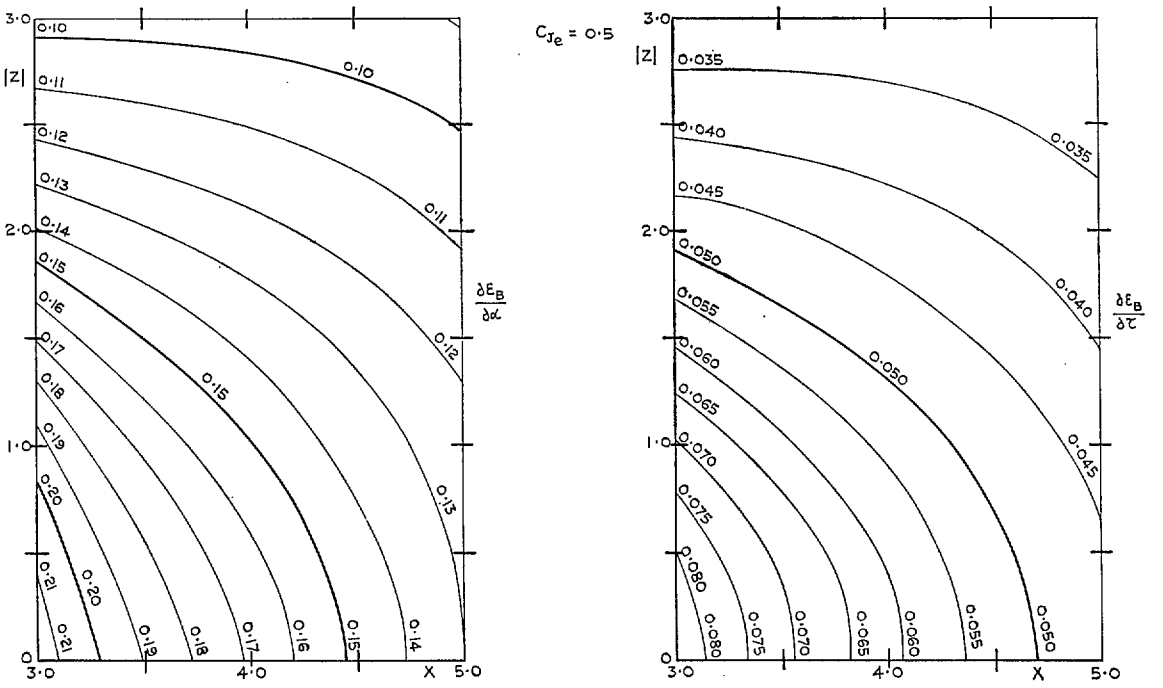

FIG. 4a. Charts for determination of downwash of infinite wing ($C_J = C_{J_e} = 0{\cdot}5$), or downwash due to bound vorticity of finite wing ($C_{J_e} = 0{\cdot}5$).

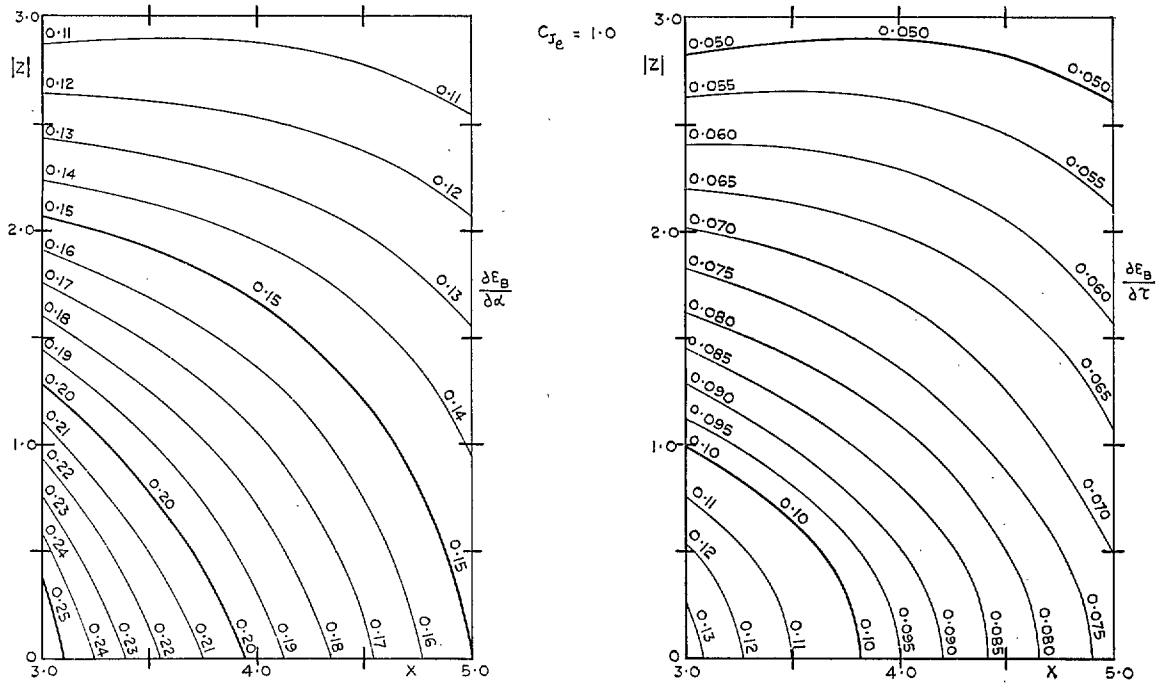

FIG. 4b. Charts for determination of downwash of infinite wing ($C_J = C_{J_e} = 1{\cdot}0$), or downwash due to bound vorticity of finite wing ($C_{J_e} = 1{\cdot}0$).

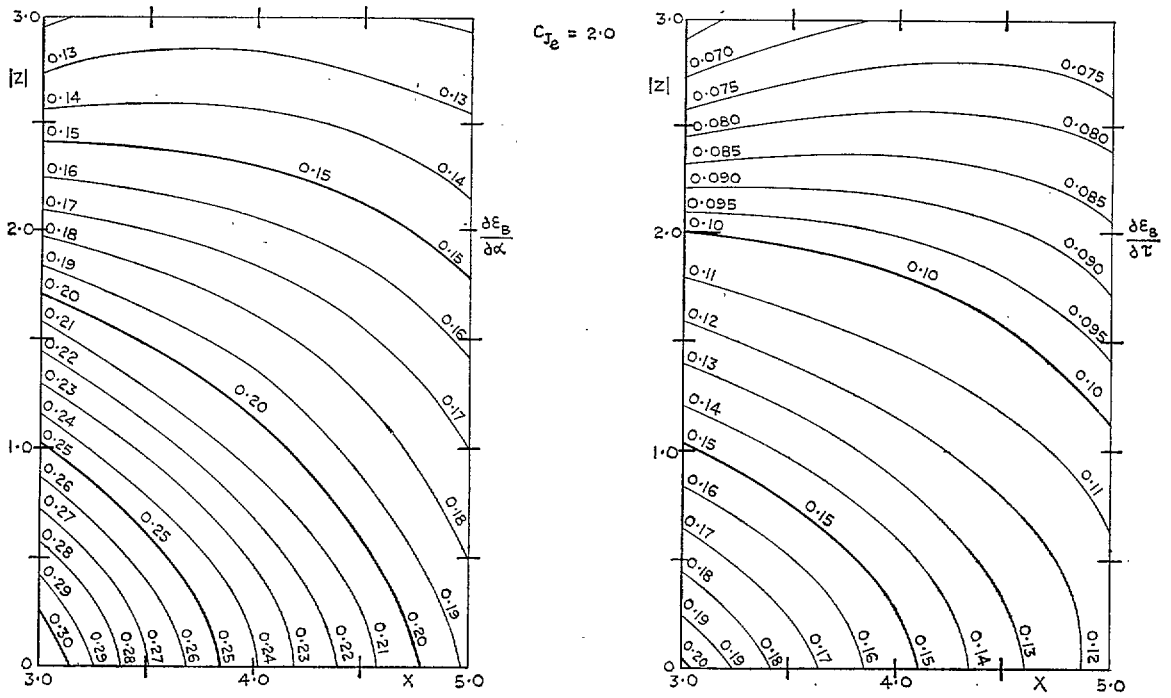

FIG. 4c. Charts for determination of downwash of infinite wing ($C_J = C_{Je} = 2{\cdot}0$), or downwash due to bound vorticity of finite wing ($C_{Je} = 2{\cdot}0$).

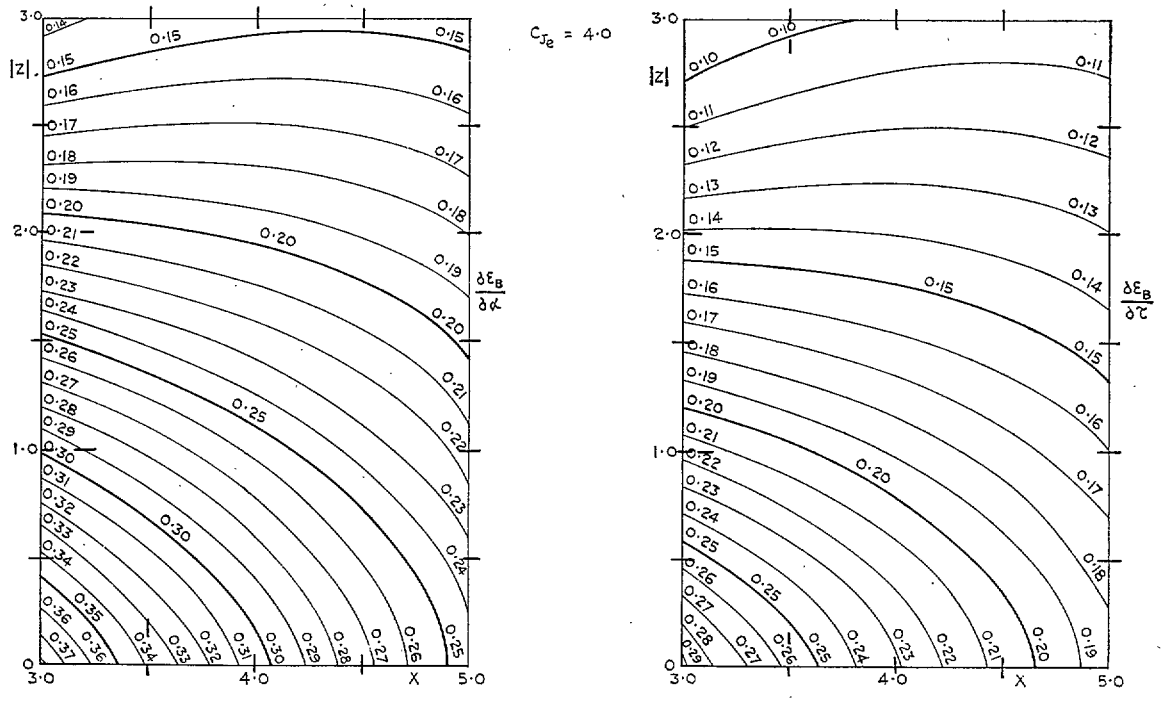

FIG. 4d. Charts for determination of downwash of infinite wing ($C_J = C_{Je} = 4{\cdot}0$), or downwash due to bound vorticity of finite wing ($C_{Je} = 4{\cdot}0$).

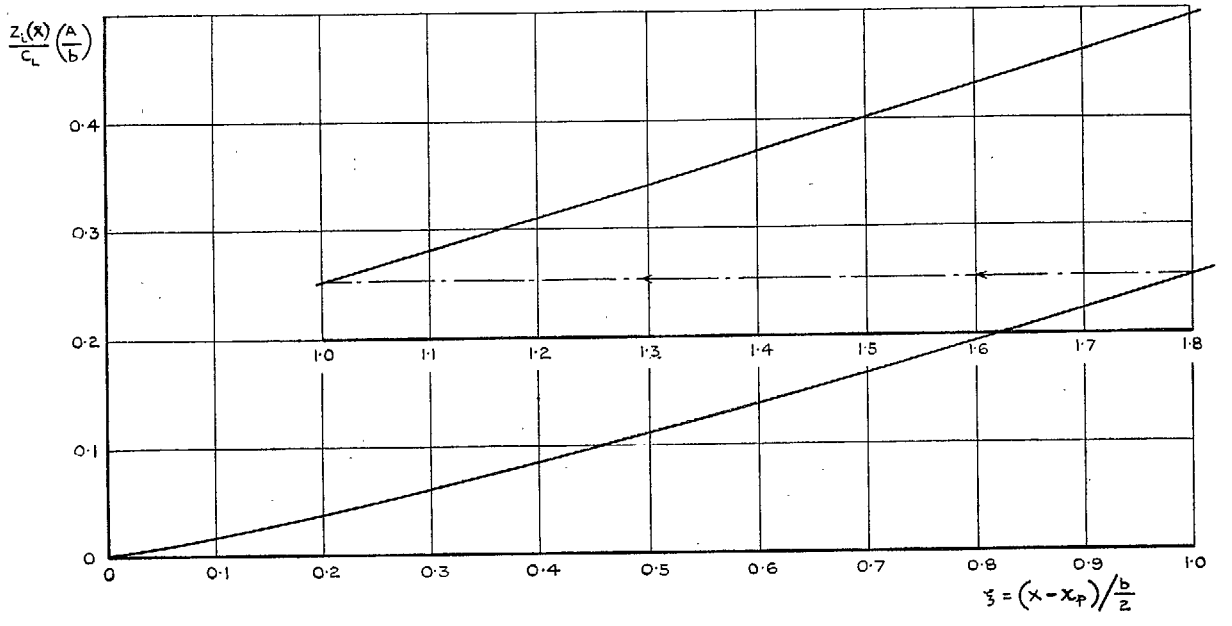

FIG. 5. Chart for determination of induced displacement of jet and wake (finite wing).

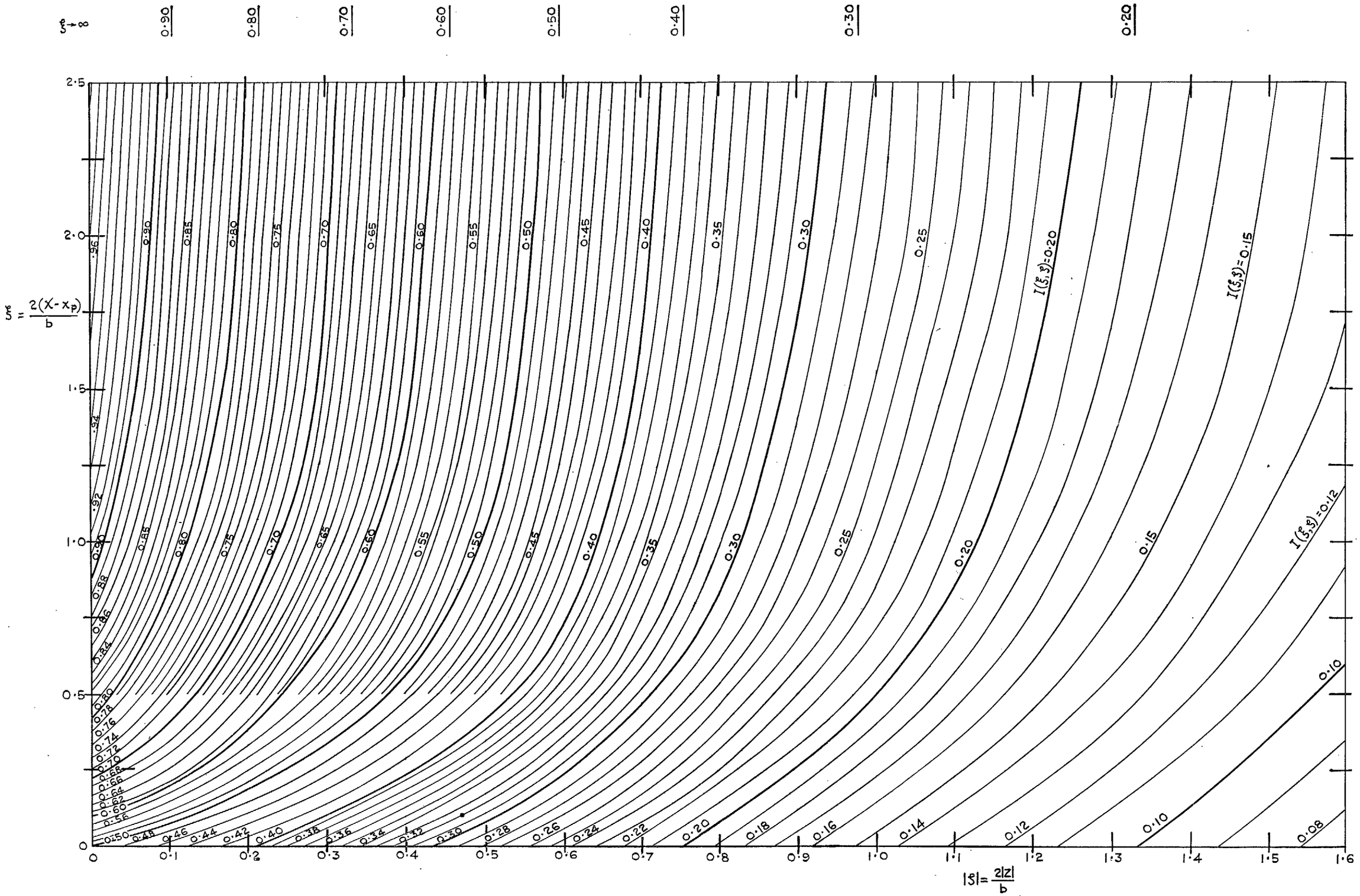

FIG. 6. Chart for determination of downwash due to trailing vortices (finite wing). $\epsilon_T = \{2C_L/(\pi A)\}\, I(\xi, \zeta)$.

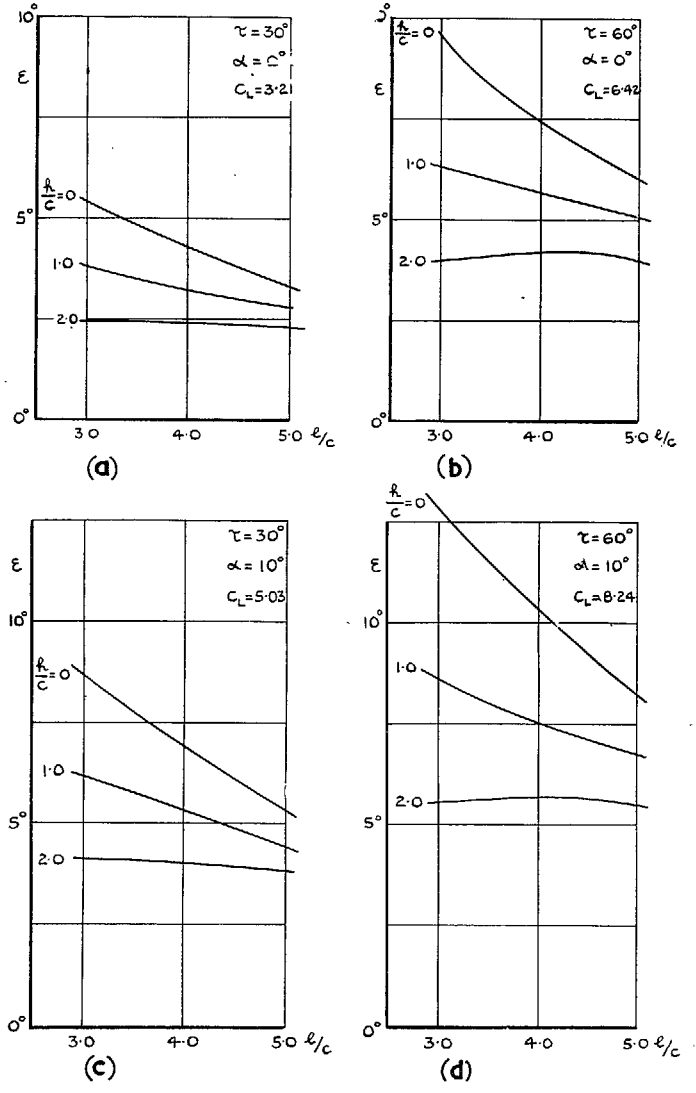

FIGS. 7a to 7d. Variation of downwash with tailplane position (Aspect ratio = ∞, $C_J = 2{\cdot}0$, $\tau = 30$ and 60 deg, $\alpha = 0$ and 10 deg).

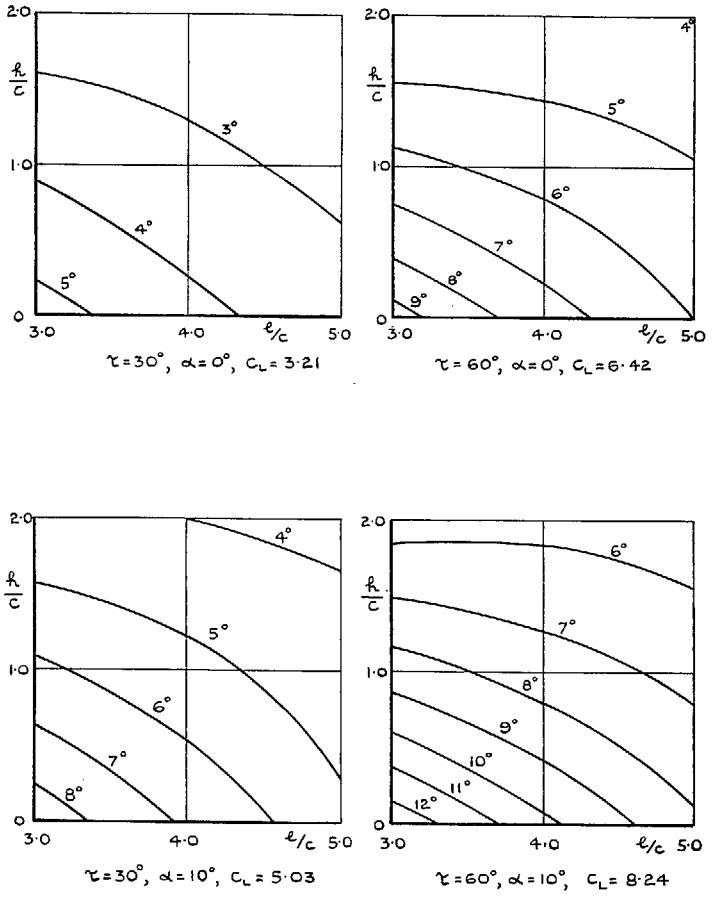

FIG. 8. Downwash field in region of tailplane (Aspect ratio = ∞, $C_J = 2{\cdot}0$, $\tau = 30$ and 60 deg, $\alpha = 0$ and 10 deg).

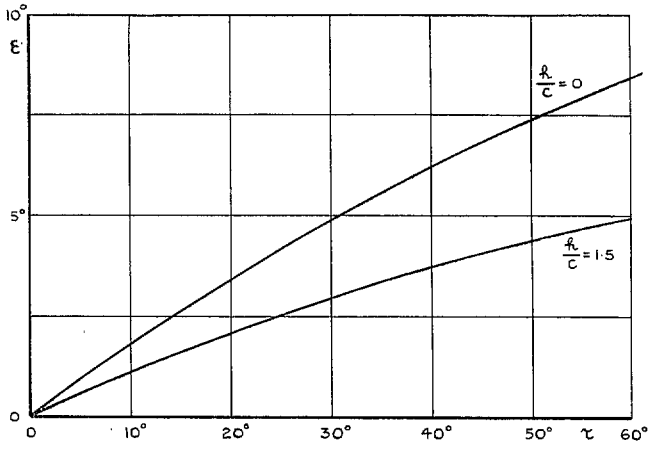

(a) VARIATION WITH JET DEFLECTION $C_J = 2{\cdot}0$

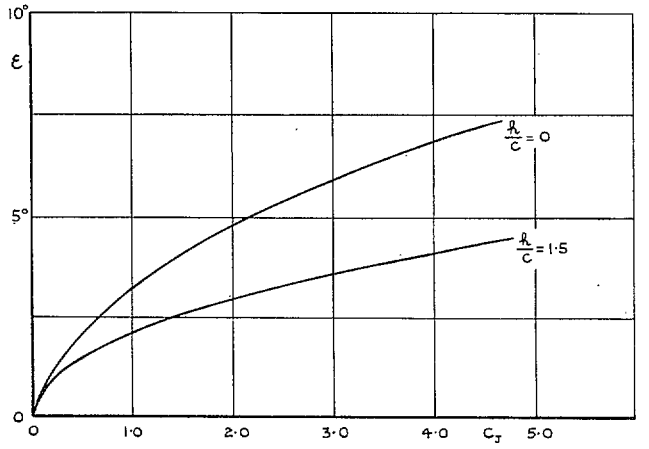

(b) VARIATION WITH JET MOMENTUM $\tau = 30°$

FIGS. 9a and 9b. Variation of downwash with jet parameters (Aspect ratio = ∞, $\alpha = 0$ deg, $l/c = 3{\cdot}5$, $h/c = 0$ and $1{\cdot}5$).

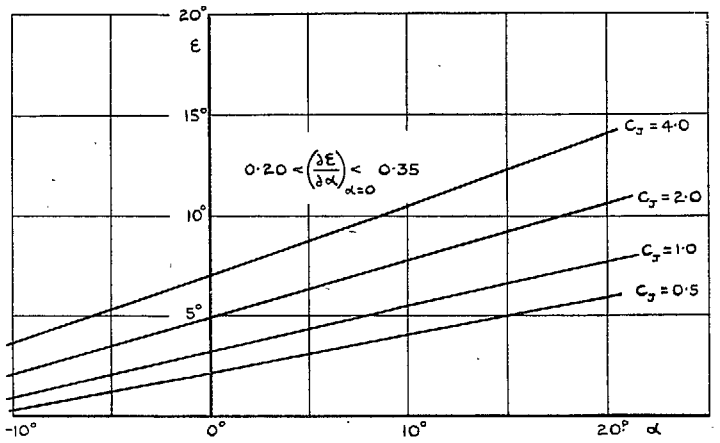

(a) $\frac{h}{c} = 0$, $\tau = 30°$

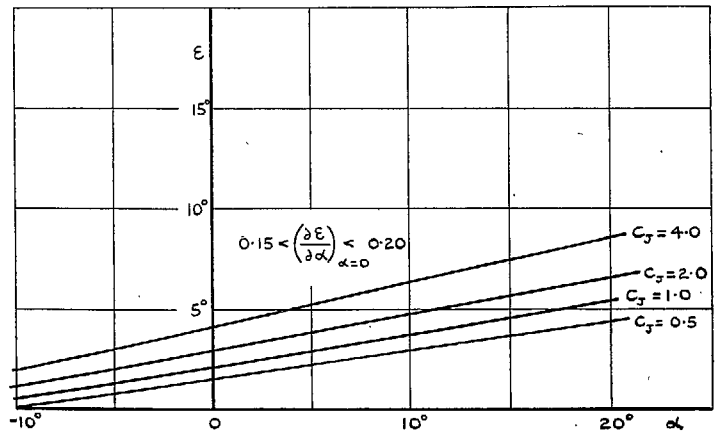

(b) $\frac{h}{c} = 1{\cdot}5$, $\tau = 30°$

FIGS. 10a and 10b. Variation of downwash with wing incidence (Aspect ratio = ∞, $l/c = 3{\cdot}5$, $h/c = 0$ and $1{\cdot}5$, $\tau = 30$ deg).

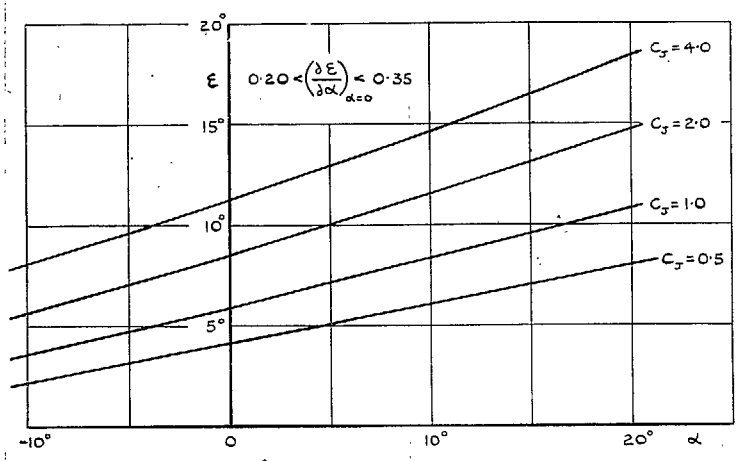

(c) $\frac{h}{c} = 0$, $\tau = 60°$

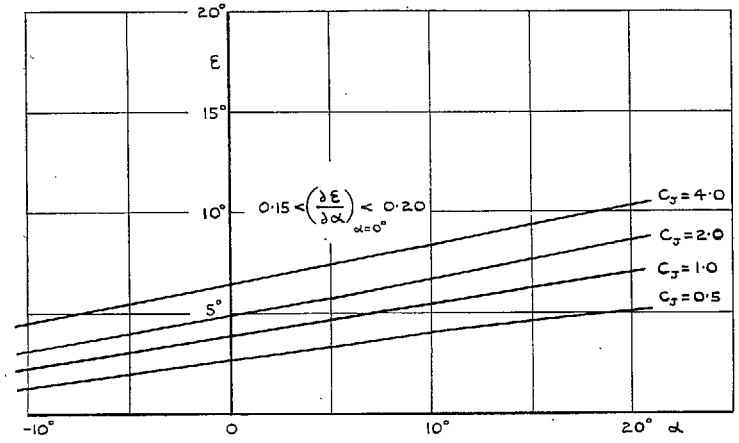

(d) $\frac{h}{c} = 1{\cdot}5$, $\tau = 60°$

FIGS. 10c and 10d. Variation of downwash with wing incidence (Aspect ratio = ∞, $l/c = 3{\cdot}5$, $h/c = 0$ and $1{\cdot}5$, $\tau = 60$ deg).

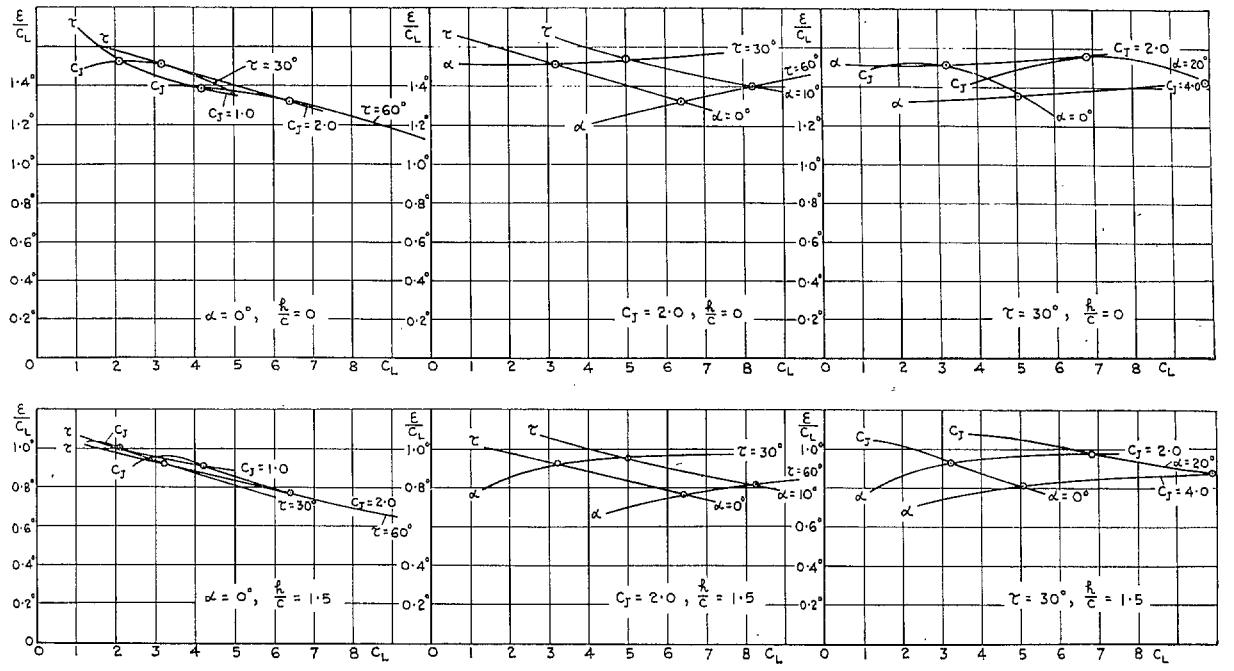

FIG. 11. Variation of ϵ/C_L with C_L, for α, C_J and τ kept constant in turn (Aspect ratio $= \infty$, $l/c = 3{\cdot}5$, $h/c = 0$ and $1{\cdot}5$).

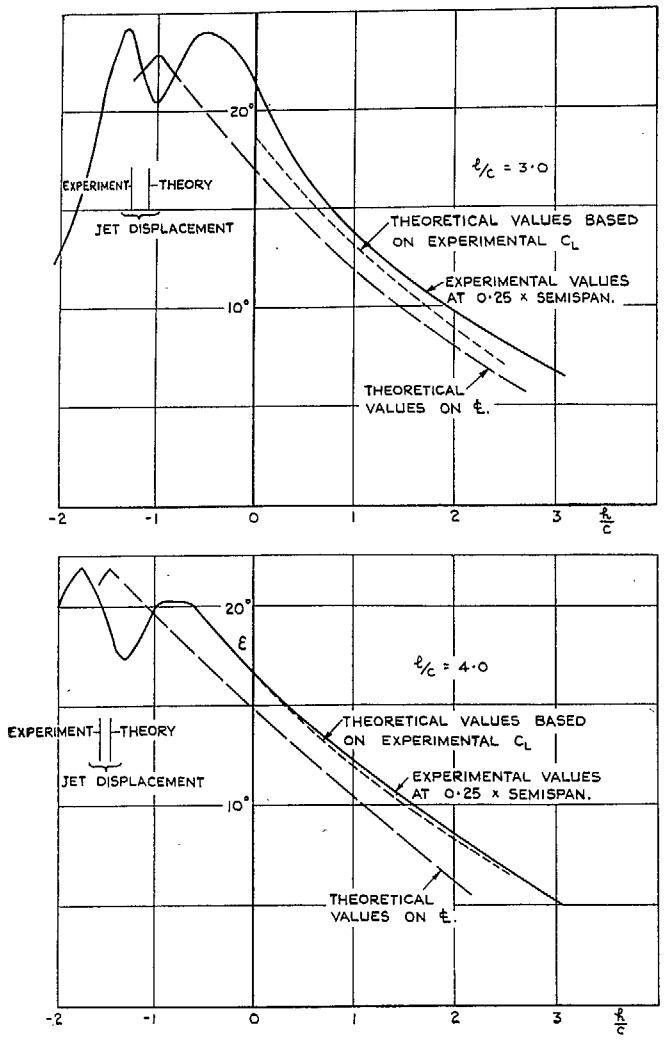

FIG. 12. Comparison between American experimental data and theoretical results (Aspect ratio = 8·4, $\alpha = 0$ deg, $C_J = 1{\cdot}6$, $\tau = 60$ deg. Experimental $C_L = 5{\cdot}2$; Theoretical $C_L = 4{\cdot}20$).

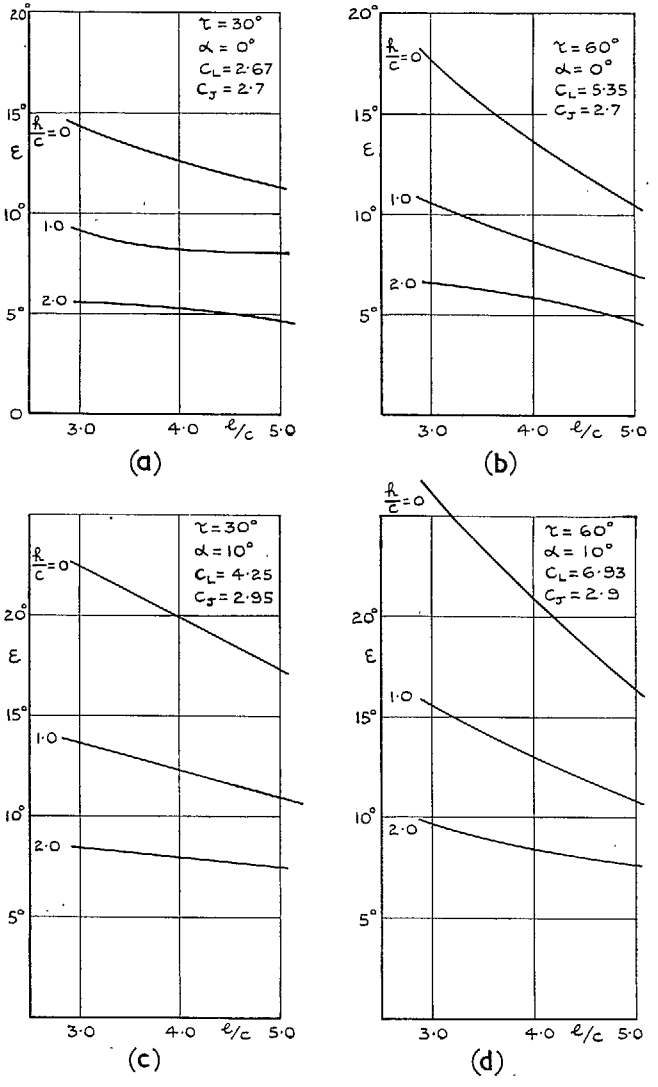

FIGS. 13a to 13d. Variation of downwash with tailplane position (Aspect ratio = 6·0, $C_J = 2{\cdot}7$ to $3{\cdot}0$, $\tau = 30$ and 60 deg, $\alpha = 0$ and 10 deg).

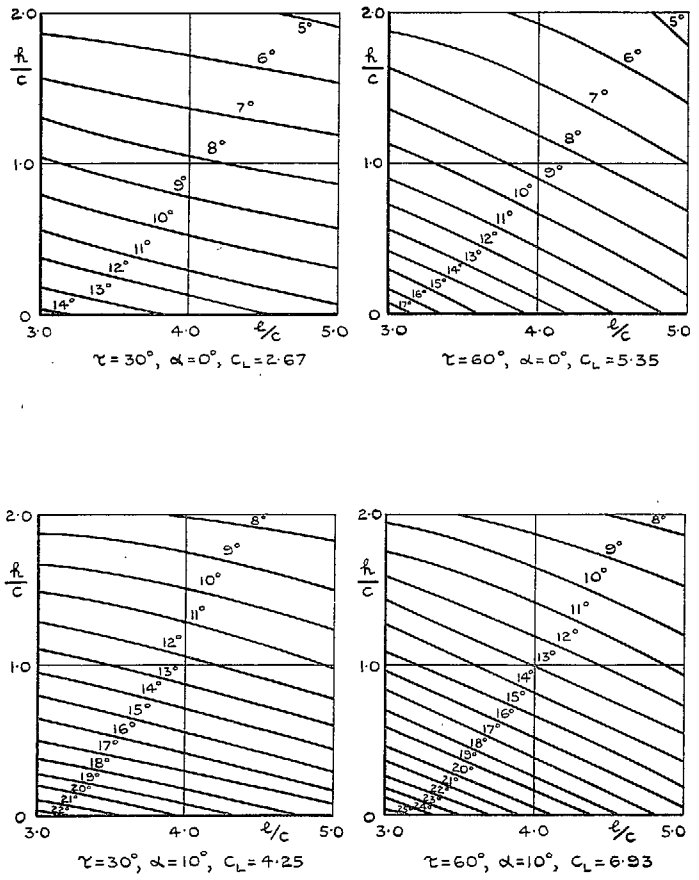

FIG. 14. Downwash field in region of tailplane (Aspect ratio = 6·0, $C_J = 2{\cdot}7$ to $3{\cdot}0$, $\tau = 30$ and 60 deg, $\alpha = 0$ and 10 deg).

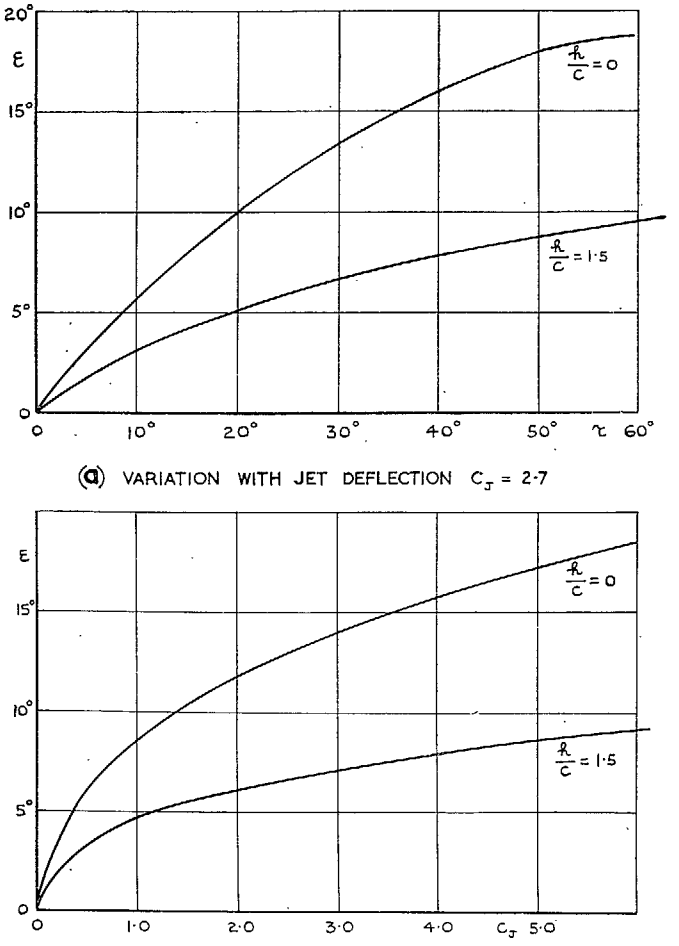

FIGS. 15a and 15b. Variation of downwash with jet parameters (Aspect ratio = 6·0, $\alpha = 0$ deg, $l/c = 3{\cdot}5$, $h/c = 0$ and $1{\cdot}5$).

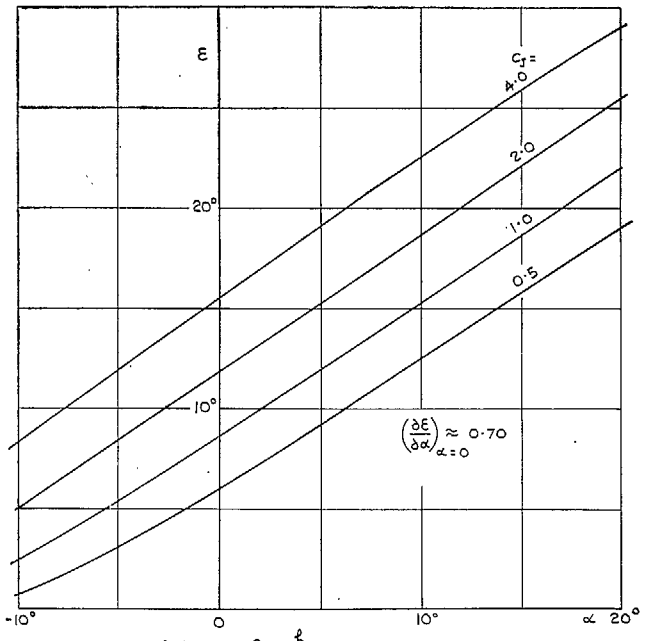

(a) $\tau = 30°$, $\frac{h}{c} = 0$

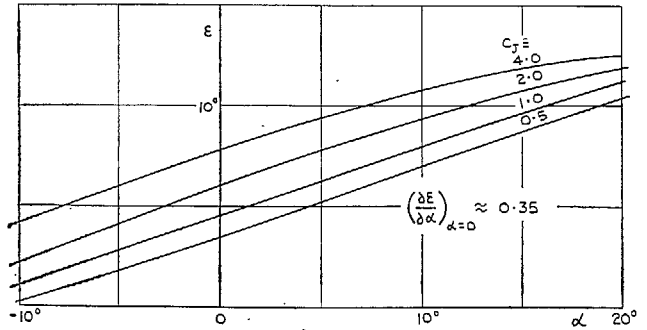

(b) $\tau = 30°$, $\frac{h}{c} = 1{\cdot}5$

FIGS. 16a and 16b. Variation of downwash with wing incidence (Aspect ratio = 6·0, l/c = 3·5, h/c = 0 and 1·5, τ = 30 deg).

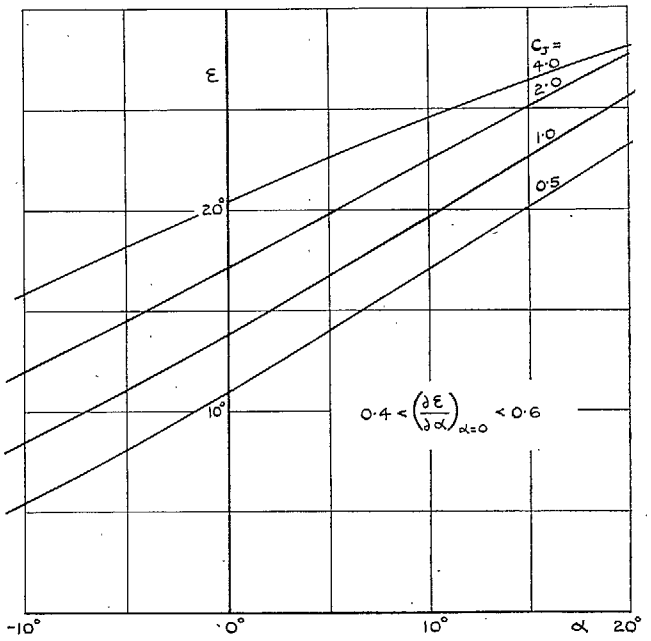

(c) $\tau = 60°$, $\frac{h}{c} = 0$

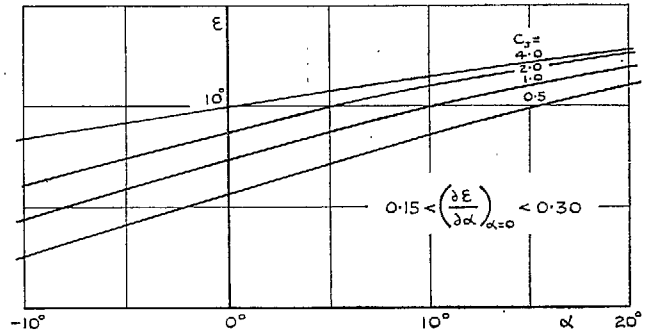

(d) $\tau = 60°$, $\frac{h}{c} = 1{\cdot}5$

FIGS. 16c and 16d. Variation of downwash with wing incidence (Aspect ratio = 6·0, l/c = 3·5, h/c = 0 and 1·5, τ = 60 deg).

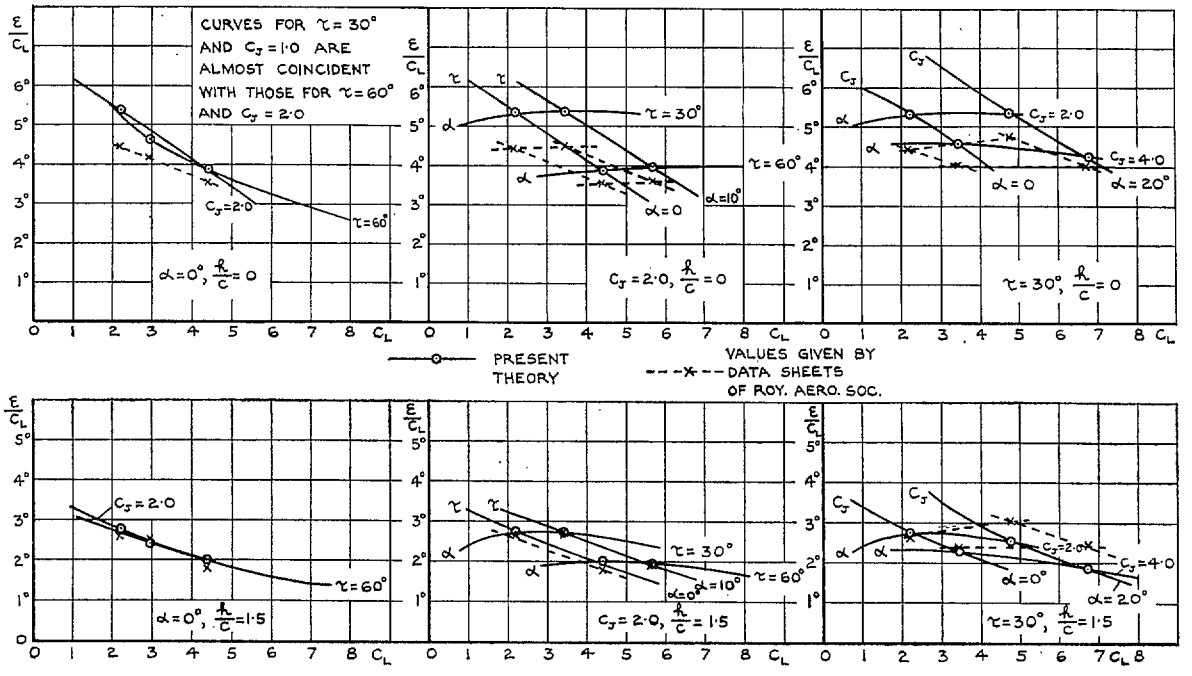

FIG. 17. Variation of ϵ/C_L with C_L, for α, C_J and τ kept constant in turn (Aspect ratio = 6·0, l/c = 3·5, h/c = 0 and 1·5).

(78824) Wt. 54/8210 K.5 2/61 Hw.

Publications of the Aeronautical Research Council

ANNUAL TECHNICAL REPORTS OF THE AERONAUTICAL RESEARCH COUNCIL (BOUND VOLUMES)

1941 Aero and Hydrodynamics, Aerofoils, Airscrews, Engines, Flutter, Stability and Control, Structures. 63*s.* (post 2*s.* 3*d.*)

1942 Vol. I. Aero and Hydrodynamics, Aerofoils, Airscrews, Engines. 75*s.* (post 2*s.* 3*d.*)
Vol. II. Noise, Parachutes, Stability and Control, Structures, Vibration, Wind Tunnels. 47*s.* 6*d.* (post 1*s.* 9*d.*)

1943 Vol. I. Aerodynamics, Aerofoils, Airscrews. 80*s.* (post 2*s.*)
Vol. II. Engines, Flutter, Materials, Parachutes, Performance, Stability and Control, Structures. 90*s.* (post 2*s.* 3*d.*)

1944 Vol. I. Aero and Hydrodynamics, Aerofoils, Aircraft, Airscrews, Controls. 84*s.* (post 2*s.* 6*d.*)
Vol. II. Flutter and Vibration, Materials, Miscellaneous, Navigation, Parachutes, Performance, Plates and Panels, Stability, Structures, Test Equipment, Wind Tunnels. 84*s.* (post 2*s.* 6*d.*)

1945 Vol. I. Aero and Hydrodynamics, Aerofoils. 130*s.* (post 3*s.*)
Vol. II. Aircraft, Airscrews, Controls. 130*s.* (post 3*s.*)
Vol. III. Flutter and Vibration, Instruments, Miscellaneous, Parachutes, Plates and Panels, Propulsion. 130*s.* (post 2*s.* 9*d.*)
Vol. IV. Stability, Structures, Wind Tunnels, Wind Tunnel Technique. 130*s.* (post 2*s.* 9*d.*)

1946 Vol. I. Accidents, Aerodynamics, Aerofoils and Hydrofoils. 168*s.* (post 3*s.* 3*d.*)
Vol. II. Airscrews, Cabin Cooling, Chemical Hazards, Controls, Flames, Flutter, Helicopters, Instruments and Instrumentation, Interference, Jets, Miscellaneous, Parachutes. 168*s.* (post 2*s.* 9*d.*)

1947 Vol. I. Aerodynamics, Aerofoils, Aircraft. 168*s.* (post 3*s.* 3*d.*)
Vol. II. Airscrews and Rotors, Controls, Flutter, Materials, Miscellaneous, Parachutes, Propulsion, Seaplanes, Stability, Structures, Take-off and Landing. 168*s.* (post 3*s.* 3*d.*)

Special Volumes

Vol. I. Aero and Hydrodynamics, Aerofoils, Controls, Flutter, Kites, Parachutes, Performance, Propulsion, Stability. 126*s.* (post 2*s.* 6*d.*)
Vol. II. Aero and Hydrodynamics, Aerofoils, Airscrews, Controls, Flutter, Materials, Miscellaneous, Parachutes, Propulsion, Stability, Structures. 147*s.* (post 2*s.* 6*d.*)
Vol. III. Aero and Hydrodynamics, Aerofoils, Airscrews, Controls, Flutter, Kites, Miscellaneous, Parachutes, Propulsion, Seaplanes, Stability, Structures, Test Equipment. 189*s.* (post 3*s.* 3*d.*)

Reviews of the Aeronautical Research Council

1939–48 3*s.* (post 5*d.*) 1949–54 5*s.* (post 5*d.*)

Index to all Reports and Memoranda published in the Annual Technical Reports

1909–1947 R. & M. 2600 6*s.* (post 2*d.*)

Indexes to the Reports and Memoranda of the Aeronautical Research Council

Between Nos. 2351–2449	R. & M. No. 2450 2*s.* (post 2*d.*)
Between Nos. 2451–2549	R. & M. No. 2550 2*s.* 6*d.* (post 2*d.*)
Between Nos. 2551–2649	R. & M. No. 2650 2*s.* 6*d.* (post 2*d.*)
Between Nos. 2651–2749	R. & M. No. 2750 2*s.* 6*d.* (post 2*d.*)
Between Nos. 2751–2849	R. & M. No. 2850 2*s.* 6*d.* (post 2*d.*)
Between Nos. 2851–2949	R. & M. No. 2950 3*s.* (post 2*d.*)

HER MAJESTY'S STATIONERY OFFICE

from the addresses overleaf

Printed and published by
HER MAJESTY'S STATIONERY OFFICE

To be purchased from
York House, Kingsway, London W.C.2
423 Oxford Street, London W.1
13A Castle Street, Edinburgh 2
109 St. Mary Street, Cardiff
39 King Street, Manchester 2
50 Fairfax Street, Bristol 1
2 Edmund Street, Birmingham 3
80 Chichester Street, Belfast 1
or through any bookseller

Printed in England

S.O. Code No. 23-3119